NEW ZEALAND JOURNAL OF GEOLOGY AND GEOPHYSICS
https://doi.org/10.1080/00288306.2022.2158881

Taylor & Francis
Taylor & Francis Group

RESEARCH ARTICLE

A time-dependent seismic hazard model following the Kaikōura M7.8 earthquake

Matthew C. Gerstenberger[a], David A. Rhoades[a], Nicola Litchfield[a], Elizabeth Abbott [a], Tatiana Goded[b], Annemarie Christophersen [a], Russell J. Van Dissen[a], Stephen Bannister[a], David Barrell[b], Zane Bruce[a], Bill Fry[a], Ian Hamling [a], Caroline Holden[a,c], Nick Horspool[a], Anna E. Kaiser[a], Yoshi Kaneko [d], Robert M. Langridge[a], Timothy A. Little[e], Biljana Lukovic[a], Sara K. McBride[f], Graeme H. McVerry[a], Andy Nicol [g], Nick Perrin[a], Jarg Pettinga[g], Mark W. Stirling [h], Chris Van Houtte[a,i] and Laura Wallace[a]

[a]GNS Science, IGNS, Lower Hutt, New Zealand; [b]GNS Science, Dunedin, New Zealand; [c]SeismoCity, Wellington, New Zealand; [d]Department of Geophysics, Kyoto University, Kyoto, Japan; [e]School of Geography, Environment and Earth Sciences, Victoria University of Wellington, Wellington, New Zealand; [f]Formerly at GNS Science, now at US Geological Survey, Menlo Park, CA, USA; [g]School of Earth and Environment, University of Canterbury, Christchurch, New Zealand; [h]Department of Geology, University of Otago, Dunedin, New Zealand; [i]Plant and Food Research, Palmerston North, New Zealand

ABSTRACT

Following the 2016 M7.8 Kaikōura earthquake, a time-varying seismic hazard model (KSHM) was developed to inform decision-making for the reinstatement of road and rail networks in the northern South Island. The source model is the sum of a gridded 100-year earthquake clustering model and an updated fault source model. The gridded model comprises long-term, medium-term and short-term components. The 100-year gridded model is constructed as the sum of 100 annual forecasts. A discounting method trades off expected earthquake occurrences of the distant future against those of the near future. The fault source model includes updates to account for newly revealed faults that ruptured in the Kaikōura earthquake and other recently obtained new information, and new time-varying probabilities of rupture for four fault segments. Two different characterisations of the Hikurangi subduction interface are incorporated via a logic tree, with weights determined by an expert panel. A suite of ground motion prediction equations contribute to a logic tree in order to account for epistemic uncertainties in source modelling for each of four tectonic region types. Here, we compare the resulting hazard estimates with the 2010 National Seismic hazard Model and recorded motions in past New Zealand and global earthquakes.

ARTICLE HISTORY
Received 29 June 2022
Accepted 7 November 2022

HANDLING EDITOR
Martin Brook

KEYWORDS
Seismic hazard; time-dependence; aftershocks; clustering; PSHA; Kaikōura earthquake

Introduction

An active period of earthquake occurrence in central New Zealand (Figure 1) began with the M_w 7.2 Darfield earthquake in September 2010. This first event in the Canterbury earthquake sequence was followed by a number of destructive earthquakes including the M_w 6.2 Christchurch earthquake of 22 February 2011. In 2013–2014 four events ranging from M_w 6.1- M_w 6.6 occurred in the Wellington region. Most recently, the 14 November 2016 M_w 7.8 Kaikōura earthquake (Kaiser et al. 2017; Woods et al. 2017) in the northern part of South Island caused large and damaging shaking around much of central New Zealand, including significant damage to national transportation infrastructure as well as a number of towns and cities. In a number of locations across Wellington city, the main shock exceeded the 10%-in-50-year design motions in the 1s–2s period range (Standards New Zealand 2004; Bradley et al. 2017). Such exceedances are a cause for concern but do not necessarily invalidate the model on which the design motions are based.

Road and rail networks on the northern South Island were severely damaged by the Kaikōura main shock, resulting in a major rebuild effort within a short time frame following the event (North Canterbury Transport Infrastructure Rebuild project; NCTIR). In New Zealand transportation infrastructure projects, such as NCTIR, are designed based on the assumption of a 100-year design life and seismic hazard estimates used for design input are consistent with this design life. In the light of the 2016 Kaikōura earthquake, and when considering the seismic activity over the last 10 or more years, statistical models of earthquake occurrence forecast increased rates of seismic activity in central New Zealand for decades to come (Gerstenberger et al. 2016; Rhoades and Christophersen 2019), and therefore must be considered during planning and rebuilding post-disaster. Through the development of a time-dependent seismic hazard model for central New Zealand, the Kaikōura Seismic Hazard Model (KSHM), this increase in seismic hazard can

CONTACT Matthew C. Gerstenberger m.gerstenberger@gns.cri.nz
Supplemental data for this article can be accessed online at https://doi.org/10.1080/00288306.2022.2158881.

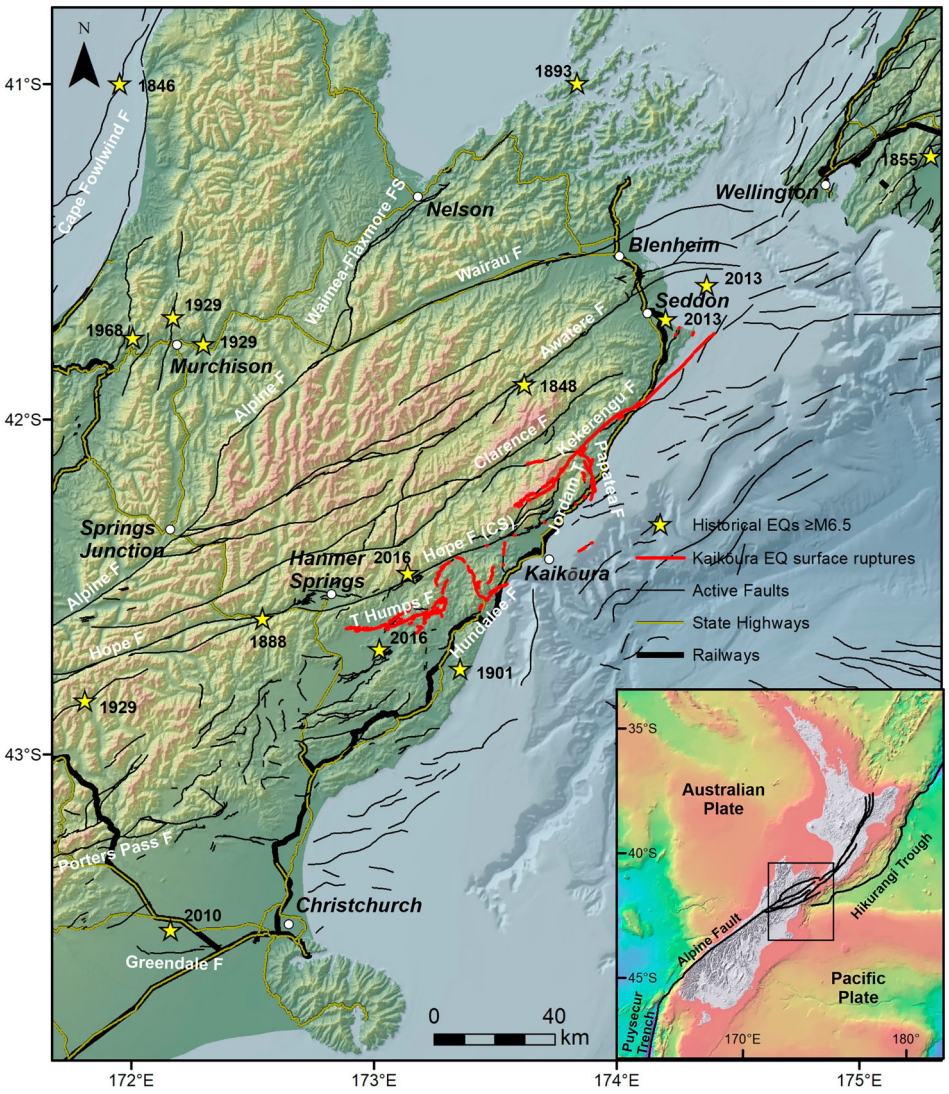

Figure 1. A, Active faults, epicentres of historical (post-1840 AD) earthquakes with $M_w \geq 6.5$ and the main road and railway networks in central New Zealand. Onshore active faults (including the Kaikōura Earthquake ground surface ruptures) are from the New Zealand Active Faults Database (https://data.gns.cri.nz/af/; Langridge et al. 2016). Selected major faults are named. Offshore active faults are from Barnes et al. (2010, 2016), Mountjoy et al. (2009), Pondard and Barnes (2010). Earthquake epicentres, labelled with the earthquake year, are from the GeoNet earthquake catalogue (https://www.geonet.org.nz/data/types/eq_catalogue). The basemaps are hillshade and digital elevation models from the 8 m 2012 LINZ (onshore; https://data.linz.govt.nz/layer/51768-nz-8m-digital-elevation-model-2012/) and the 250 m 2016 NIWA bathymetry (offshore; https://data-niwa.opendata.arcgis.com/datasets/nz-bathymetry-250m-imagery-raster-layer/explore) datasets. **B,** Plate boundary setting of central New Zealand. CSHM is the area of the Canterbury Seismic Hazard Model (Gerstenberger et al. 2014, 2016).

be considered for all infrastructure rebuild projects, including NCTIR.

The KSHM is a model built during earthquake response and recovery in order to meet the immediate needs of a quickly-moving recovery effort. Model development during response and recovery necessitates a huge amount of work, including testing, in an extremely short time frame. To accomplish this we started with forecasting models already in use for 11 previous large earthquakes and the initial response to Kaikōura over the seven years from 2009 to 2016, including the Canterbury seismic hazard model (Canterbury SHM). The KSHM has been constructed by building upon the developments initially laid out for the Canterbury SHM – a time-dependent seismic hazard model developed in response to the Canterbury earthquake sequence (Gerstenberger et al. 2014, 2016). As with the Canterbury SHM, the KSHM applies the same probabilistic seismic hazard analysis (PSHA) framework as the New Zealand National Seismic Hazard Model (NSHM; Stirling et al. 2002, 2012), but replaces some of the component models with those developed or revised specifically for the seismic situation initiated by this earthquake sequence. We have not attempted to develop a new model for all of New Zealand at this time but have developed a model applicable to central New Zealand alone (Figure 1).

Within the KSHM there are two basic classes of models: (1) a source model, consisting of the sum of a gridded time-varying earthquake clustering model

and the fault source model; and (2) the ground motion prediction model. Each of these basic model classes consists of a collection of component-models and have been revised since the 2010 NSHM and Canterbury SHM were published (Stirling et al. 2012; Gerstenberger et al. 2014, 2016). Similar to the Canterbury SHM and NSHM the source model components (clustering model and fault source model) are complementary and contribute to the forecast at all time scales.

One new challenge faced in developing the KSHM was the need to consider the possibility of the Hikurangi subduction zone rupturing south of Cook Strait (Figure 1). In the 2000 and 2010 NSHMs (Stirling et al. 2002, 2012), both of which included modelling of the Hikurangi subduction zone, the possibility of rupture occurring on the interface south of Cook Strait was explicitly excluded, based on work by Reyners and Eberhart-Phillips (2009). Whether or not rupture occurred on the plate interface during the Kaikōura main shock is still controversial (e.g. Bai et al. 2017; Hamling et al. 2017; Holden et al. 2017; Wallace et al. 2018; Wang et al. 2018; Mouslopoulou et al. 2019; Hamling 2020); however, given the possibility that it may be seismogenic and due to observed afterslip that can be resolved to a broader interface zone (Wallace et al. 2017), it is important that sources representing subduction interface rupture south of Cook Strait are included in the KSHM. This is discussed further in Section 3.6.

Kaikōura gridded time-varying clustering model

The 100-year gridded time-varying clustering model developed for the KSHM is a hybrid and is similar in many ways to the hybrid clustering model that was constructed for the Canterbury region of New Zealand following the 2010 Darfield and 2011 Christchurch earthquakes (Gerstenberger et al. 2014, 2016; Rhoades et al. 2016). However, in a departure from what was done for Canterbury, the Kaikōura model has separate short-term and medium-term time-varying components instead of just a single combined time-varying component. Also, the long-term time-invariant component of the clustering model now includes information on strain rates as well as past earthquakes – the first time that geodetic observations have been included in such a direct way in operational earthquake forecasts in New Zealand.

The hybrid clustering model component of the KSHM comprises three main components: a short-term time-varying component, a medium-term time-varying component, and a long-term time-invariant component. Each component itself comprises multiple models (as described below). They each take the form of a regional earthquake likelihood model (RELM; Schorlemmer and Gerstenberger 2007), which is a forecast of the number of shallow (hypocentral depth <40 km) earthquakes expected to occur in spatial cells on a 0.05-degree square grid, within magnitude bins of width 0.1 units, and within time bins as described below. The lowest magnitude bin covers the magnitude range from 4.95 to 5.05, and the highest magnitude bin covers the range from 7.95 to 8.05.

The 100-year forecast for the clustering model starts on 1 December 2017, a date guided by the NCTIR project goal to reopen regional transport infrastructure just over one year following the Kaikōura mainshock and is based on the earthquake catalogue up to 1 May 2017. It thus has a 7-month time-lag from the end of the available catalogue. It is constructed as the sum of 101 separate forecasts for separate time-periods (and time-lags): a one-month forecast beginning on 1 December 2017, a set of annual forecasts beginning on 1 January each year from 2017 through to 2116, and an 11-month forecast commencing 1 January 2117. The short-term time-varying component is computed only for the first 25 years, and the medium-term time-varying component only for the first 50 years. Thus, in the first 25 years, the hybrid clustering model forecast in each space-magnitude bin is defined as the maximum of the forecasts of the short-term, medium-term, and long-term time-invariant components in that bin. Between 25 and 50 years the hybrid forecast is defined as the maximum of the medium-term and long-term components. For periods beyond 50 years, the hybrid is equal to the long-term time-invariant component.

The use of a bin-by-bin maximum between a time-varying and long-term component was first introduced in the Short-term Earthquake Probabilities (STEP) model (Gerstenberger et al. 2004, 2005) and was also applied in the Canterbury SHM. The main difference in the Kaikoura model is that it has short-term and medium-term components instead of a single time-varying component. The maximum combination makes sense in this context because the contributions from the time-varying components are relatively short-lived. An advantage of the maximum combination, as opposed to the alternative of using a weighted average, is that it gives full weight to the three conceptually distinct components of seismicity. A possible disadvantage is that it could result in over-estimation of the 100-year earthquake rate. However, given that there is appreciable uncertainty in the total long-term rate of distributed seismicity, this possible over-estimation does not seem unreasonably large. Although the uncertainty in the 100-year rate of distributed seismicity is not explicitly assessed here, we aim to minimise the uncertainty in each of the components by averaging over two or more available models in each class.

Short-term time-varying clustering component

The short-term component of the gridded time-varying clustering model is constructed as a 50:50 weighted average of two standard aftershock clustering models, which aim only to forecast earthquakes triggered by previous earthquakes, i.e. clusters of aftershocks. Aftershocks occur after almost all large earthquakes, and also after many smaller earthquakes. The expected number of aftershocks is highest immediately after an earthquake and thereafter decays like a power-law in time. The decay of aftershock rates is referred to as the Omori-Utsu law (Utsu et al. 1995) and forms the basis for modelling aftershock occurrence.

The two short-term forecasting models we have used are the STEP model (Gerstenberger et al. 2004, 2005), which was used by the US Geological Survey for automatic online forecasting for a number of years and is installed in the Collaboratory for the Study of Earthquake Predictability (CSEP) testing centres in New Zealand, California, and Italy, and a version of the ETAS (Epidemic Type Aftershock Sequence) model (Ogata 1988; Harte 2013, 2015, 2016, 2019).

Both the STEP and ETAS models aim to forecast the aftershocks of all earthquakes, not just the aftershocks of the Kaikōura mainshock, in the input catalogue, which is updated as new earthquakes are added. However, the key differences between the STEP and ETAS models are in the mathematical set-up and in how the parameters are derived. The STEP model also produces direct estimates of earthquake rates, while the ETAS model produces numerous simulated catalogues from which the rate forecasts are derived. Although these two models have a similar aim and basis and often produce similar forecasts, they can also differ appreciably at certain times and locations. For example, during the Kaikōura aftershock sequence the ETAS model has tended to produce lower forecasts of earthquake rates within the aftershock area than the STEP model. This difference arises because, given the parameter settings of the two models, the ETAS model expects large earthquakes to trigger fewer aftershocks and small earthquakes to trigger more aftershocks than does the STEP model. Incomplete detection of early aftershocks in the catalogue, which is well-known to occur following major earthquakes (Christophersen et al. 2017), may also contribute to this difference. However, subsequent investigations have shown that both the STEP and ETAS models tended to over-estimate the number of earthquakes in the first two years of the Kaikoura aftershock sequence (Rhoades et al. 2018; Harte 2019).

Medium-term time-varying clustering component

The medium-term component of the gridded time-varying clustering model uses the EEPAS (Every Earthquake a Precursor According to Scale) model (Rhoades and Evison 2004). The EEPAS model is based on an increase in the rate of occurrence and magnitude of minor earthquakes observed to occur prior to the occurrence of major earthquakes. Associated with this precursory scale increase are predictive scaling relations (Evison and Rhoades 2002, 2004).

The EEPAS model assumes that the precursory scale increase phenomenon occurs at all scales in the seismogenic process. It does not distinguish precursory earthquakes from others, simply regarding every earthquake as a precursor of larger events to follow it. Each earthquake makes a transient contribution to the estimate of future earthquake occurrence in its surroundings. The mean of the magnitude distribution of that contribution is about one unit higher than the magnitude of the earthquake. The mean of the time distribution increases with the magnitude of the precursor, by about a factor of three for each additional magnitude unit. For example, the contribution from a magnitude 4 earthquake peaks 2–3 years after its occurrence but extends for more than a decade, and the contribution from a magnitude 5 earthquake peaks about 8 years after its occurrence and extends for several decades. The contribution from a magnitude 7.8 earthquake would thus peak about two centuries after its occurrence and extend for about a millennium. The spatial distribution of the contribution occupies an area that also increases with the magnitude of the earthquake.

The EEPAS model has been applied to a number of regional earthquake catalogues and consistently forecasts major earthquakes better than time-invariant models (Rhoades and Evison 2005, 2006; Console et al. 2006; Rhoades 2007). EEPAS is generally more informative at high magnitudes than at lower magnitudes (Rhoades 2011), and a mixture between EEPAS and an aftershock model is more informative for forecasting with short-to-medium time horizons than either of its components alone (Rhoades and Gerstenberger 2009; Rhoades 2013). For transparent testing, the EEPAS model has also been installed in CSEP earthquake forecast testing centres in New Zealand (Gerstenberger and Rhoades 2010), Japan (Rhoades 2011), and California (Schneider et al. 2014). The EEPAS model is also a contributor to the Canterbury SHM (Gerstenberger et al. 2014, 2016; Rhoades et al. 2016).

The medium-term component is constructed as a 50:50 weighted average of two versions of the EEPAS model: one with every earthquake weighted equally, and the other with aftershocks down-weighted (Rhoades and Evison 2004). These two versions of EEPAS often give similar forecasts, but during aftershock sequences the equal-weighted version tends to forecast higher rates than the version with aftershocks down-weighted. The version with equal weighting

tends to perform better when the target magnitude threshold is relatively low, such as 5.0 as it is in the present case (Schneider et al. 2014). However, there is some evidence that the version with aftershocks down-weighted performs better at higher target magnitudes (Rhoades and Evison 2004, 2005, 2006; Rhoades 2011).

Long-term time-invariant component

The long-term component of the clustering model is time-invariant, i.e. the forecast does not change from year to year, and is developed by taking a weighted average of three different time-invariant models known as NSHMBG, PPE-SSR, and PPE1950 as further explained below.

NSHMBG

The NSHMBG model is the background seismicity model from the 2010 update of the New Zealand National Seismic Hazard Model (2010 NSHM; Stirling et al. 2012). It is a smoothed seismicity model with a 50-km Gaussian smoothing kernel, with rates based on a declustered catalogue, since it is designed to forecasts mainshocks only.

PPE-SSR

The PPE-SSR model is a multiplicative hybrid of three components: a spatially uniform baseline model, a smoothed seismicity model known as PPE, and a gridded map of shear strain rate in New Zealand computed from the Global Positioning System (GPS) observations over the period 1991–2011. The development of PPE-SSR is described in detail by Rhoades et al. (2017), who fitted and retrospectively tested a large number of possible multiplicative models to the New Zealand region.

Starting with a spatially uniform Poisson baseline model (SUP), Rhoades et al. (2017) evaluated the information gains of multiplicative hybrids incorporating selected combinations of covariates formed from two smoothed seismicity models and six other gridded variables in a fitting period and a testing period. The PPE-SSR model was the multiplicative hybrid model that performed best in the testing period.

The smoothed seismicity models included in the hybrid modelling by Rhoades et al. (2017) were NSHMBG and the Proximity to Past Earthquakes (PPE) model. The other covariates included were: Proximity to Mapped Faults (PMF), which measures the proximity of any cell to all points on mapped faults, weighted by their estimated slip rates; Proximity to the Plate Interface (PPI), which measures the proximity of a cell to any point on the Australian-Pacific plate interface through New Zealand; the Shear Strain Rate (SSR), Rotational Strain Rate (RSR) and Dilatational Strain Rate (DSR), which were computed by J. Beavan using the method of Beavan and Haines (2001); and a binary fault variable, which took the value 1 if a fault intersected a cell, and 0 otherwise. Rhoades et al. (2017) showed that the strain rate covariates were more informative than the others, that SSR was the most informative individual covariate, and that any hybrid model including SSR was more informative than any model that excluded it.

The PPE component of the PPE-SSR model was described by Rhoades and Evison (2004) and is based closely on a model proposed by Jackson and Kagan (1999). PPE adopts the assumption that earthquakes above a given magnitude threshold will continue to occur close to the locations where they have occurred in the past, and especially near to the locations of previous large earthquakes. It incorporates spatial smoothing of the locations of past earthquakes with an inverse power-law kernel, weighted by earthquake magnitude, and includes a small spatially uniform background term to allow for surprises. The PPE model rates are designed to forecast all earthquakes, including aftershocks and other clustered activity, above the minimum magnitude threshold of 4.95.

PPE1950

The PPE model relies on a complete catalogue above its minimum target magnitude threshold m_c for its fitting. PPE1950 is a version of the PPE model that uses the early period of the earthquake catalogue up to 1950. The early catalogue from 1840 to 1950 contains much information on the locations of large earthquakes in New Zealand that is not included in our models fitted with $m_c = 4.95$. The PPE1950 model uses the New Zealand earthquake catalogue up to 1950 with $m_c = 5.95$. For use at lower magnitudes, it is extrapolated down to magnitude 5.0 based on the Gutenberg-Richter frequency-magnitude relation. The PPE1950 model was included in the long-term component of the Canterbury SHM (Gerstenberger et al. 2014, 2016; Rhoades et al. 2016).

Weighting the short-term, medium-term and long-term model components

The weights accorded to the short-term, medium-term and long-term components of the 100-year clustering model component of the KSHM were based mostly on retrospective testing over a 26-year period from 1986 to 2012, similar to the testing of the Canterbury clustering model and its individual components, described by Rhoades et al. (2016). Further testing and fitting over the same time-period has been used to support the judgements involved in the setting of weights for the Kaikōura clustering model. As well as the gridded time-varying clustering models used

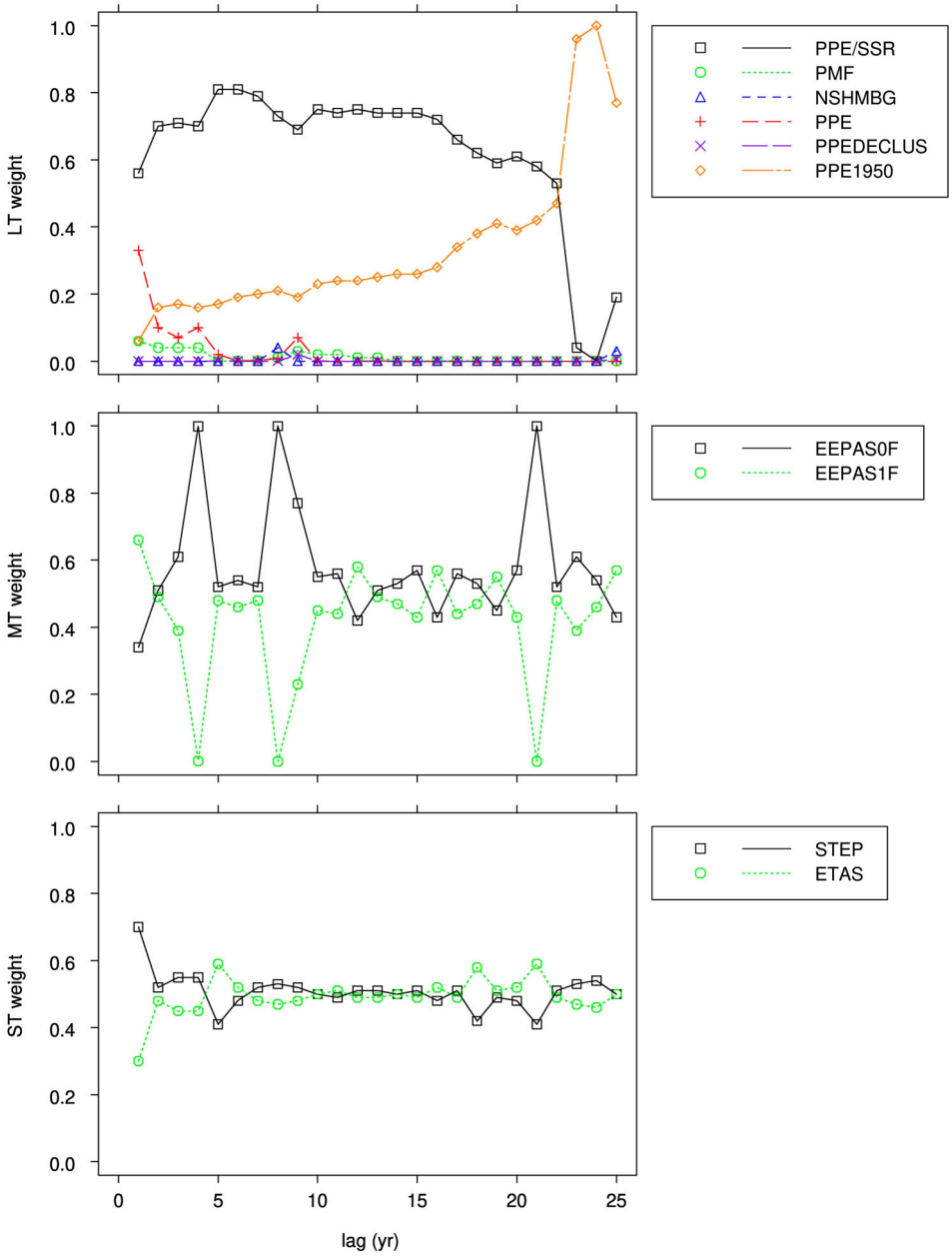

Figure 2. Optimal weights for models in the long-term (LT), medium-term (MT) and short-term (ST) components of the hybrid model fitted to the earthquake catalogue of the CSEP New Zealand testing region over the period 1981–2012. The models are input as a set of one-year forecasts with time-lags ranging from 1 to 25 years. The optimal model weights are calculated using all forecasts with the same time-lag. The sum of the weights in each component is constrained to be 1. Note that only one time-invariant annual forecast was used for the PPE-SSR, PPE1950 and PMF models. All other models were used in multiple versions, using the data up to the appropriate date for the lagged forecasts.

in the Canterbury study, the further testing included the PPE-SSR and PMF models in the long-term component. PMF performed well in earlier additive and multiplicative hybrid modelling (Rhoades and Stirling 2012; Rhoades et al. 2015)

The recent fitting (Figure 2) has shown that a high weighting (0.5) of the PPE-SSR model is beneficial to the long-term component as is moderate weighting of PPE1950 (0.3), especially at longer time-lags (10–25 years), as shown in the top panel of Figure 2. Four long-term models considered and tested (NSHMBG, PPE, PMF, and PPEDECLUS – a version of PPE with aftershocks down-weighted) do not contribute much to the optimal fit at any time-lag. The weight of 0.2 accorded to the NSHMBG model recognises that it is the sole contributor to the existing, solely time-invariant distributed/background model of the 2010 NSHM (Stirling et al. 2012). Its retention as a component of the present model is desirable for that reason.

The equal-weighting of models in the short – and medium-term components is well-supported by the optimisation results shown in Figure 2. In both of these components, neither model is consistently dominant over the other across all time-lags, though one or other of the models dominates the optimal weighting at different, varying time-lags.

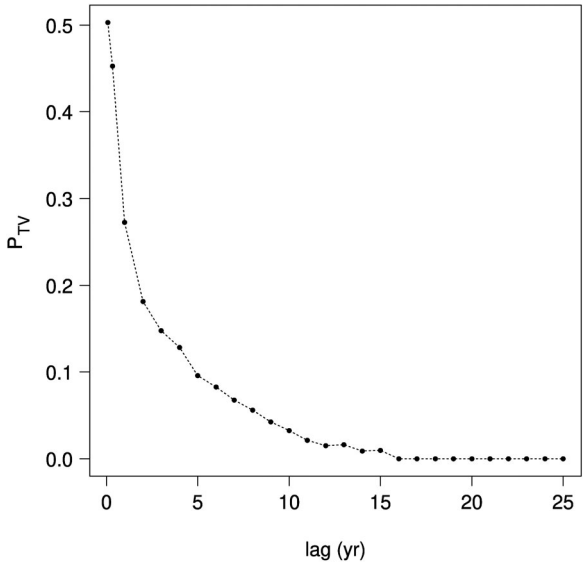

Figure 3. Proportion P_{TV} of the total expected number of earthquakes in the hybrid model contributed by the time-varying (short-term and medium-term) components, as a function of the time lag, within the CSEP New Zealand testing region (Gerstenberger and Rhoades 2010) over the fitting period 1986–2012.

Time-varying contribution to forecasts

The contribution of the short-term and medium-term components to the hybrid forecast is expected to diminish with increasing time-lag. One way of measuring this contribution is by the proportion P_{TV} of the total expected number of earthquakes contributed by the time-varying components at any given time-lag:

$$P_{TV} = \frac{E(N)_{Hybrid} - E(N)_{LT}}{E(N)_{Hybrid}} \quad (1)$$

where $E(N)_{Hybrid}$ and $E(N)_{LT}$ are the expected numbers of earthquakes under the clustering model and its long-term component, respectively. The manner in which P_{TV} diminishes as the time-lag increases in the 26-year fitting period is shown in Figure 3. The contribution of the time-varying components is more than 50% in a 3-month model with 1-month time-lag and is zero for time-lags greater than 15 years to two significant figures. However, the proportional contribution is not the same at all magnitudes. The longevity of the contribution from time-varying models is expected to increase with increasing magnitude because of the increase in precursor time with magnitude observed in the EEPAS model. A 15-year time horizon is similar to the precursor time for a magnitude 7 earthquake. Earthquakes larger than about magnitude 5.5 contribute to the future time-varying rate at magnitudes above 7 for longer than 15 years but make only a minor contribution to the overall expected number of earthquakes for magnitudes above 5.

Information gain due to time-varying components

The information gain per earthquake I_{TV} due to the time-varying components of the 100-year clustering model can be estimated from the difference of the natural log likelihood of the clustering model from the natural log likelihood of its long-term component, divided by the number of target earthquakes. That is:

$$I_{TV} = \frac{\ln L_{Hybrid} - \ln L_{LT}}{N} \quad (2)$$

where L_{Hybrid} and L_{LT} are the likelihoods of the hybrid clustering model and its long-term component, respectively, and N is the number of target earthquakes. The log likelihood of a regional earthquake likelihood model was defined by Schorlemmer et al. (2007) based on the discrete Poisson assumption. A different definition given by Rhoades et al. (2011) is used here: the sum over target earthquakes of the log expected number of earthquakes in associated bins minus the total number of earthquakes expected over all bins. This is based on a discrete approximation of the continuous point process log likelihood, which avoids the unrealistic Poisson assumption. The difference between these two approaches does not affect information gain statistics.

The pattern of decrease in I_{TV} as the time-lag increases in the 26-year fitting dataset is shown in Figure 4. Starting from 0.7 at a time-lag of 1 month, I_{TV} rapidly diminishes until a time-lag of 2 years and approaches zero at a time-lag of about 10 years.

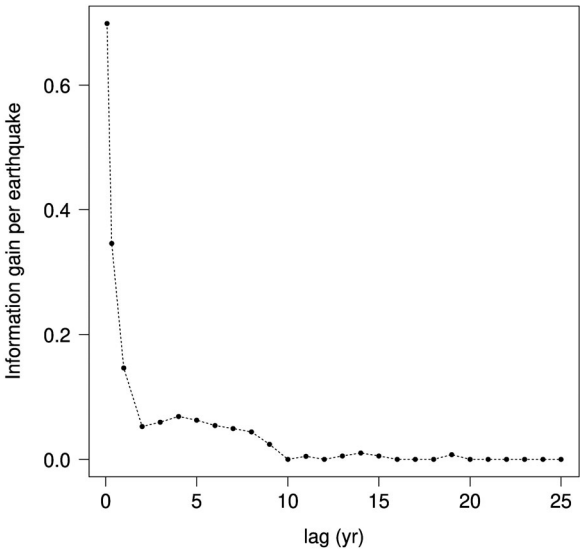

Figure 4. Information gain of adding time-varying (short-term and medium-term) components to the distributed seismicity model, as a function of time lag, within the CSEP New Zealand testing region (Gerstenberger and Rhoades 2010) over the fitting period 1986–2012.

Equivalent constant forecast rates

We have implemented a method for quantifying equivalent constant rates from time-varying hazard forecasts, as proposed in section 4.2 of Yeo and Cornell (2005). The method applies a discount rate to trade-off expected earthquake occurrences of the distant future against those of the near future, as a basis for working out the equivalent constant rate. The discount is relevant to deciding the amount that should be invested now to counter the effects of expected future earthquakes. From equation (4.6), p.67 of Yeo and Cornell (2005), we infer the following definition of the equivalent constant annual rate *ECAR* in a space-magnitude bin k of the 100-year clustering model forecast:

$$ECAR(k) = \alpha \exp(-\alpha \tau_i) r_i(k) \qquad (3)$$

where α is the discount rate, $r_i(k)$ is the expected number of earthquakes in the bin k during the ith forecast period, and τ_i is the time between the present (taken as 1 December 2017) and the beginning of the ith forecast period. We have applied a discount rate of 6%, consistent with New Zealand Treasury guidelines for infrastructure (2020).

For a forecast that decreases from a relatively high value to a constant value, as in the 100-year clustering model component, the equivalent constant annual rate is higher than the average annual forecast rate but lower than the annual forecast rate in the first few years.

Conversion of forecasts from M_L to m_w

The 100-year clustering model component produces forecasts of local magnitude M_L, but our ground motion models require moment magnitude M_w as input. The forecasts of M_L have been converted to forecasts of M_w using the approximate bin-by-bin conversion formula with assumed Gutenberg-Richter b-value of 1, described by Rhoades and Christophersen (2017). The approximate conversion formula is based on a regression of M_w on M_L fitted to a homogeneous subset of the earthquake catalogue and allows for expected deviation of individual points from the regression line and corrects for the bias due to uncertainties in the M_w values. Rhoades and Christophersen (2017) showed the observed difference of the b-value from 1 and typical uncertainties in M_L, derived from information in the earthquake catalogue, are small enough to have a negligible effect on the conversion. Using the regression parameters given by Christophersen et al. (2017), the conversion formula is:

$$\frac{r_w(m_i)}{r_L(m_i)} = A \exp(B + C m_i + D m_i^2) \qquad (4)$$

where $r_w(m_i)$ is the expected number of earthquakes in a magnitude bin for M_w centred on magnitude m_i in a given spatial cell, $r_L(m_i)$ is the expected number of earthquakes in the corresponding magnitude bin for M_L, $A = 0.9137$, $B = -1.506$, $C = 0.1687$ and $D = 3.018 \times 10^{-3}$.

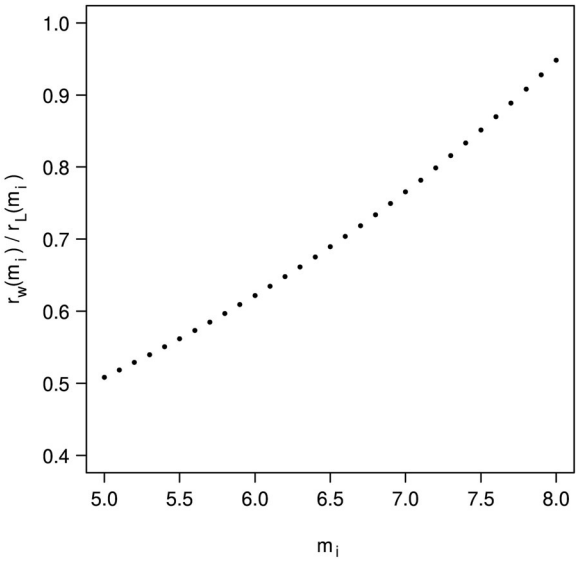

Figure 5. Ratio of expected numbers of earthquakes in M_w and M_L bins as a function of the magnitude m_i at the center of the bin. Based on Equation (4).

The conversion ratio is plotted in Figure 5. The ratio of $r_w(m_i)$ to $r_L(m_i)$ is 0.51 for $m_i = 5.0$, and increases as m_i increases, to be 0.95 for $m_i = 8.0$. Therefore, overall, the expected rates in the forecasts for M_w are lower than those in the forecasts for M_L.

Proportional contributions of clustering model components

The contributions of the time-varying components are more long-lasting in the Kaikoura forecast than the New Zealand-wide analysis in the fitting period would suggest. During a major active aftershock sequence, the proportional contribution of the time-varying component (the bin-by-bin maximum of the short – and medium-term components) to the hybrid clustering model may be expected to be greater at a given time-lag than that shown in Figure 3, because of the relatively high concentration of large earthquakes. In the ETAS model, the larger a mainshock is, the more aftershocks it is expected to have and in the EEPAS model, the larger a precursory earthquake is, the longer the precursor time is expected to be. Figure 6 shows the proportion P_{TV} for the first 50 years of the Kaikoura 100-year clustering model. It can be verified that P_{TV} is higher for a given time-lag in Figure 6 than in Figure 3; whereas P_{TV} drops to zero after 16 years in Figure 3, it remains above zero out to 50 years in Figure 6. Also shown in Figure 6 is the proportion P_{LT} of the clustering model that is provided uniquely by the long-term component,

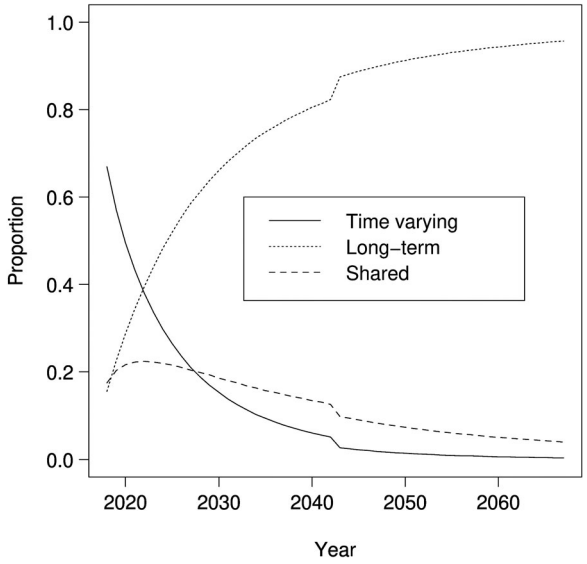

Figure 6. Proportional unique contributions, P_{TV} and P_{LT}, of the time-varying component and long-term component, respectively, to the Kaikōura hybrid 100-year distributed seismicity model, as a function of time. Also shown is the proportion P_S of the forecast that is shared in common between the time-varying and long-term components.

defined by

$$P_{LT} = \frac{E(N)_{Hybrid} - E(N)_{TV}}{E(N)_{Hybrid}} \quad (5)$$

and the proportion P_S that is shared in common between the time-varying (maximum of short – and medium-term) and time-invariant (long-term) components of the clustering model, given by

$$P_S = 1 - P_{TV} - P_{LT}. \quad (6)$$

P_S can also be viewed as the proportion of the expectation contributed by a model defined as the minumun of the time-varying and long-term components in each bin. P_{LT} is much below P_{TV} initially but increases with time to be close to one after 50 years. P_S is a significant proportion of the total clustering model forecast, and actually exceeds P_{TV} after about 10 years. The step in the curves in between 2042 and 2043 is due to the termination of the short-term component after 25 years.

It is worth noting that the implementation of ETAS used in the Kaikoura model is different from the one used in optimal fitting to the period 1986–2012. This difference could contribute in a minor way to the differences seen between Figures 6 and 3.

A similar analysis of the proportional contributions, P_{ST} and P_{MT} of the short – and medium-term components, respectively, to the total time-varying component of the clustering model is shown in Figure 7. P_{ST} is initially slightly higher than P_{MT}, but after the first year P_{MT} exceeds P_{ST}. The proportion shared in common by the short-term and medium-term components is consistently about 0.3 throughout the 25 years over which the short-term component contributes to the clustering model. The gradual increase of P_{ST} after about 10 years, after initially declining, can be attributed to the long tail of the Omori-Utsu power law for aftershock rate decay in the models contributing to the short-term component. In contrast, the medium-term models have contributions which are distributed as lognormal in time. The lognormal distribution is not as long-tailed as a power law and as such, the contributions from small earthquakes in the magnitude range 3–4 reach their peak after 1–3 years and are declining strongly through the tail of their time distribution by 10 years.

Fault source model

The fault source model component of the KSHM source model, relative to that of the 2010 NSHM, has been updated to take into account: (1) faults which were not previously in the 2010 NSHM that ruptured to the ground surface in the 2016 Kaikōura earthquake; and (2) new information obtained since the compilation of fault sources for the 2010 NSHM. The total number of fault sources in the KSHM is 569, compared with 541 in the 2010 NSHM. The locations of new and modified fault sources in the northern South Island are shown in Figure 8, the parameters are contained in Supplement 1, and descriptions of changes to individual fault sources are in Supplement 2. In this section, we first summarise the method used to update the fault sources and the key changes made. We then outline the calculation of conditional probabilities of rupture for three faults with the best paleoseismic data: the Kekerengu, Hope, and Awatere faults (further detail is

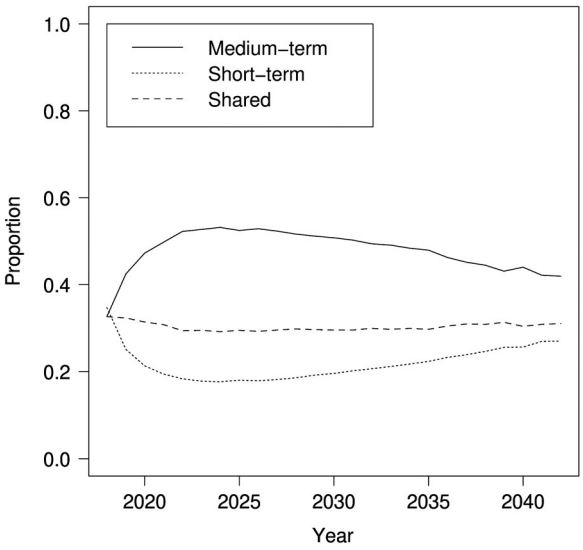

Figure 7. Proportional unique contributions, P_{ST} and P_{MT}, of the short-term and medium-term components, respectively, to the combined time-varying component of the Kaikōura hybrid distributed seismicity model, as a function of time. Also shown is the proportion P_S of the forecast that is shared in common between the short-term and medium-term components.

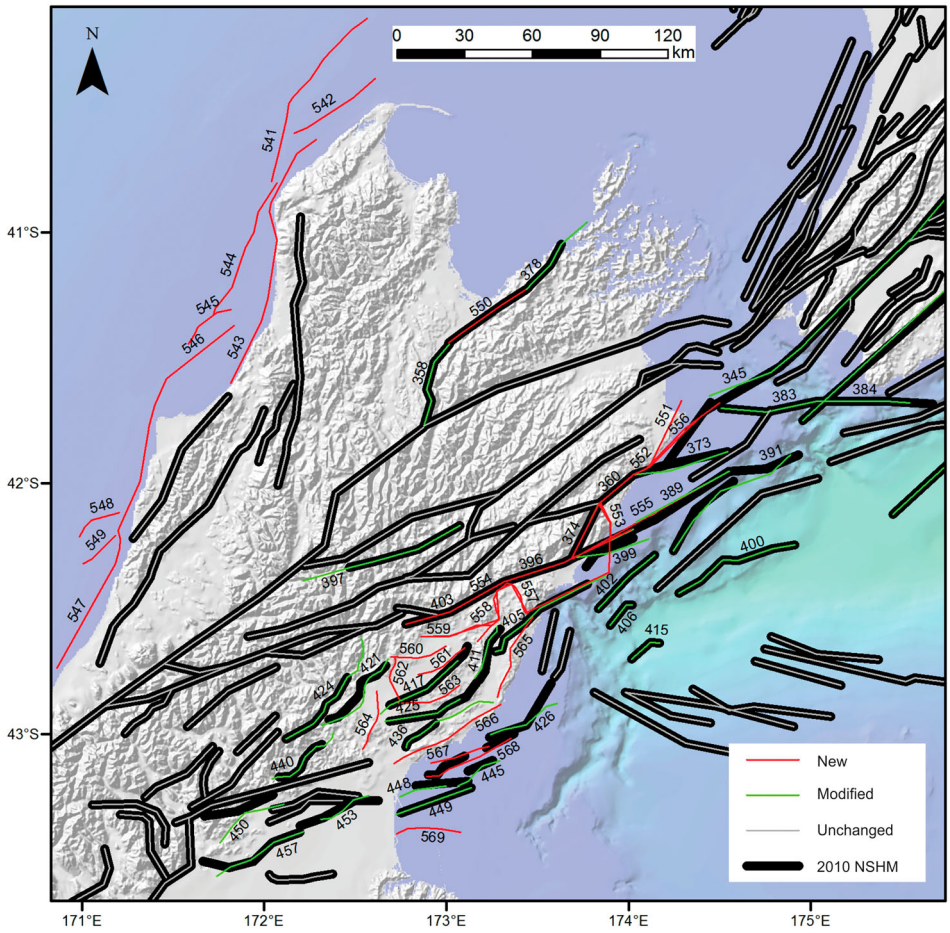

Figure 8. A comparison of the central New Zealand fault sources in the KSHM (red, green, grey thin lines) with those in the 2010 NSHM (black bold lines). The fault sources that have been added (new) or modified are numbered, and their parameters are given in Electronic Supplement 1 and the changes are described for each source in Electronic Supplement 2. The Hope Fault and Jordan-Kekerengu-Needles-Chancet multi-fault sources are shown in Figure 9.

presented in Supplement 3), followed by description of the changes made to the parameterisation of the fault sources representing the Hikurangi subduction interface.

Fault source method

The methodology to compile the KSHM fault sources is the same as that used in the 2010 NSHM (Stirling et al. 2012). The fault source geometries are rectangular discrete planes with length L determined from surface or subsurface information, with dip and dip directions determined from geological or geophysical data (Supplement 2), and with the basal seismogenic depth determined from the depth distribution of seismicity. Basal seismogenic depths have not been reviewed and revised for the KSHM and depths for new fault sources have been inferred to be the same as adjacent sources. The top seismogenic depth is defined as 0 km if there are surface traces or, for blind faults, at depths inferred from geophysical or geological data. Maximum magnitude M_{max} is calculated from regressions of moment magnitude M_w on fault area A (calculated from L and down-dip width W). The regression used for all of the new or modified sources is:

$$M_w = 4.18 + (2/3)\log W + (4/3)\log L \quad (7)$$

Recurrence interval RI (for all faults except the Kekerengu, Hope, and Awatere faults) is calculated from:

$$RI = D/SR \quad (8)$$

where D is single-event-displacement (mm) and SR is slip rate (mm/yr). SR is from paleoseismic data or estimated as described in Supplement 2. D is calculated from seismic moment M_o using the equation of Aki and Richards (1980):

$$M_o = \mu LWD \quad (9)$$

where μ is the rigidity modulus (assumed to be 3×10^{11} dyn/cm^2). As for the 2010 NSHM, D is assumed to be the average coseismic surface displacement. Calculated D and RI values are compared to paleoseismic data, and if they don't match within uncertainties, then L is altered by splitting or combining sources. Overlapping sources (segment options) have been included for a limited number

of faults and are here referred to as multi-fault sources.

Summary of key fault source updates

In this section we summarise the updates to fault sources in the northern South Island from the 2010 NSHM; further details are contained in electronic supplements 1 and 2. They are grouped into two categories: (1) sources that ruptured in the 2016 Kaikōura earthquake; and (2) sources located in geographic areas near to the Kaikōura rupture where there has been significant new work undertaken since the fault source model component of the 2010 NSHM was compiled. These updated fault sources (individual faults only, not the multi-fault sources) were subsequently incorporated into version 1.0 of the New Zealand Community Fault Model (Seebeck et al. 2022).

2016 Kaikōura earthquake surface rupture fault sources

The 2016 Kaikōura earthquake was notable for its complexity and the number of faults which ruptured (Nicol et al. 2016; Clark et al. 2017; Hamling et al. 2017; Holden et al. 2017; Kearse et al. 2018; Langridge et al. 2018; Litchfield et al. 2018; Williams et al. 2018; Ando and Kaneko 2018; Zinke et al. 2019; Hamling 2020; Howell et al. 2020). These included faults that were not previously recognised as active or were identified after the compilation of fault sources for the 2010 NSHM (e.g. Barrell and Townsend 2012).

Six new fault sources have been added to represent faults that had major (>1.5 m) surface displacement during the Kaikōura earthquake. The Humps (559), Leader (558) and Stone Jug (557) fault sources are in North Canterbury, and the Leader fault source is a composite source encompassing three short faults – the South Leader, North Leader, and Conway-Charwell faults (Barrell and Townsend 2012; Nicol et al. 2016). Farther north, the Papatea Fault (553) (Langridge et al. 2018) is included as a new individual fault source, as well as part of a multi-fault source in combination with the Hope and Kekerengu faults . The London Hill Fault (551) did not rupture to the ground surface in the Kaikōura Earthquake (Litchfield et al. 2018) but is now included to represent minor surface ruptures on nearby, subparallel, previously-unrecognised faults. A new multi-fault source (2016KaikEqke – 556) encompassing all the faults with maximum surface displacement of >1.5 m (The Humps, Leader, Stone Jug, Hundalee (part), Papatea, Jordan, Kekerengu and Needles faults) has also been added (Figure 9A). The M_{max} for the 2016KaikEqk is fixed at M_w 7.8, the mean of published values for the Kaikōura Earthquake (e.g. Kaiser et al. 2017).

Modifications were made to the existing Hundalee fault source (405) and some other multi-fault sources

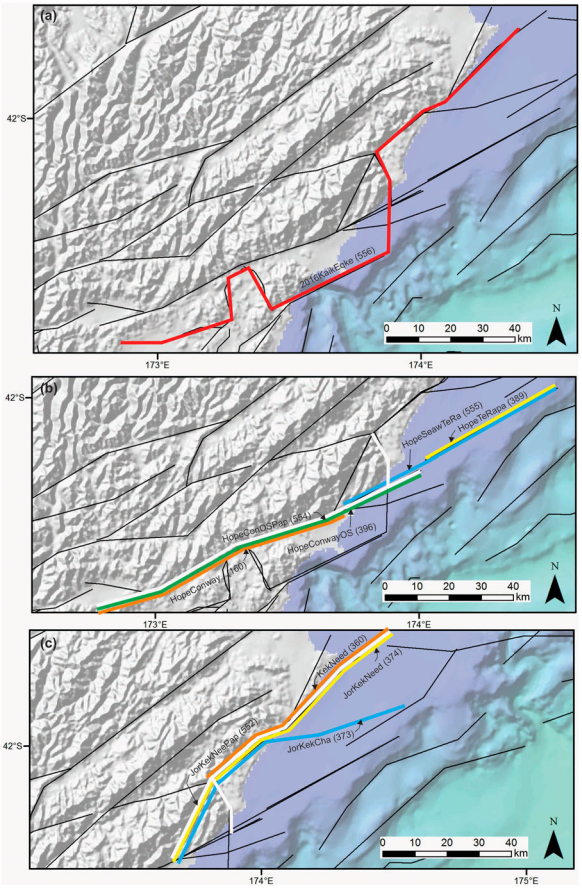

Figure 9. Multi-fault sources that have been added or modified in the KSHM. **A,** The 2016KaikEqke source, encompassing all the major surface ruptures in the Kaikōura Earthquake. **B,** Hope Fault section multi-sources. **C,** Jordan-Kekerengu-Needles-Chancet multi-fault sources. The source locations in (B) and (C) are shown adjacent to each other for clarity purposes, but in reality are the same (i.e. on top of each other). The numbers refer to the parameter table in Electronic Supplement 1 and each source is described in Electronic Supplement 2.

in light of information from the Kaikōura Earthquake surface ruptures (Williams et al. 2018). The Hundalee fault surface rupture extended offshore beyond where previously mapped, so the source was lengthened to reflect the inferred extent. The multi-fault sources changes are described in the multi-fault sources section.

Offshore North Canterbury and Southern Marlborough

Significant new mapping and active fault characterisation has been undertaken in the offshore North Canterbury and southern Marlborough areas (Wallace et al. 2012; Barnes et al. 2015, 2016, unpublished data), partly in response to the ongoing Canterbury earthquake sequence. From this data, thirteen fault sources have had their locations, slip rates, and in some cases dips updated using new, high-resolution bathymetric and seismic reflection survey data. These include the Boo Boo fault sources (BoobooAll – 383; BoobooEast – 384) and the southern end of the

Wairarapa – Nicholson fault source (WairarapNich – 345) in southern Cook Strait, the onshore-offshore KaikōuraMS05 fault source (399) in North Canterbury, and nine fault sources in the North Canterbury shelf and slope areas (MS01 – 402; MSO2 – 406; MS04 – 400; MS09 – 415; NorthCant4 – 445; NorthCant8 – 426; Pegasus1nw – 449; UpperSlope – 391; Waikuku – 448).

Additionally, three new fault sources have been added in Pegasus Bay (Figure 8). The CenPeg1n2 source (569) represents three short submarine faults, the LeithNC1137 (568) four faults, and the MotNthCant5 (567) two faults (Barnes et al. 2016).

North Canterbury (onshore)

A series of regional-scale compilations of active faults and folds have been undertaken for the entire Canterbury Region, including those by Barrell and Townsend (2012), Barrell (2013), Barrell and Begg (2013), Barrell and Van Dissen (2014), Barrell (2015) and Litchfield et al. (2019) that cover parts of the northern South Island. From this work, seven new fault sources have been added and 11 fault sources have been updated.

The new fault sources are situated in North Canterbury (Figure 8). The Doctors (564), Balmoral (562), McCulverden (560), LeonardMound (561), and Alexander (563) faults are all situated around or within the Culverden Basin, south of The Humps Fault which ruptured in the Kaikōura earthquake. The Doctors fault source represents three faults and an anticline (Barrell and Townsend 2012). The AmberlBlythe (565) and Hawkswood (565) fault sources are within the coastal ranges and represent several blind faults considered responsible for uplift of the ranges (Barrell and Townsend 2012).

Modifications to the locations, slip rates, and in some cases, dips have been made to the Hororata (457), SpringfldView (450), Springbank17 (453), LeesV2017 (440), Esk2017 (424), Waitohi2017 (421), OmihiLwrHuru (436), KaiwaraS2017 (425), Lowry2017 (417), and KaiwaraN2017 (411) fault sources. The Fowlers fault source (397) has also been lengthened to the west.

Offshore North Westland

The 2010 NSHM contained no fault sources offshore of the South Island's West Coast north of Milford Sound. Subsequent interpretation of seismic reflection data has shown the presence of a number of active faults lying 2–30 km offshore of north Westland (Hokitika to Cape Farewell, Figure 8) (Barnes and Ghisetti 2016). These have been characterised into nine active fault sources: Kahurangi (541), Farewell (542), Kongahu (543), CFF4 (544), CFF3 (545), CFF2 (546), CFF1 (547), Razorback (548), and Elizabeth (549). The CFF sources are segments of the Cape Farewell Fault. The locations and parameters of these nine new North Westland fault sources are taken directly from Barnes and Ghisetti (2016).

Waimea fault

In the 2010 NSHM, the Waimea-Flaxmore Fault System (Ghisetti et al. 2020) was represented by two approximately equal-length active fault earthquake sources called WaimeaS and WaimeaN. Subsequent paleoearthquake trenching investigations (A. Nicol, unpublished data) show that the most recent rupture of the southern portion of the fault system was more recent than that further north near Nelson. This suggests that the southern portion of the fault system is a separate earthquake source compared to the portion closest to Nelson. This has led to the definition, in the KSHM, of a revised-length (shortened) fault source called WaimeaS (378), a new source called WaimeaC (550), and a revised-length (shortened) source called WaimeaN (358) (Figure 8).

Multi-fault sources

The 2010 NSHM included six multi-fault sources, which comprise combinations of two or more faults or fault sections. As a result of both the Kaikōura earthquake surface ruptures and the new mapping in offshore North Canterbury, several modifications were made to multi-fault sources encompassing sections of the Hope Fault and combinations of the Jordan, Kekerengu, Needles, and Chancet faults (Figure 9B,C). The JorKekNeed (374) multi-fault source ruptured in the Kaikōura earthquake (Kearse et al. 2018; Litchfield et al. 2018).

Two new sources and one modified single source are now included in the Hope Fault section multi-sources (Figure 9B). The two new sources are the HopeConOSPap (554), which includes the Papatea Fault, and the HopeSeawTeRa source (555), which encompasses the Seaward and Te Rapa sections of the Hope Fault. The previous HopeTeRapa1n2 source has been shortened and is now included as the HopeTeRapa (389) source. The northeast end of the HopeConwayOS (396) source has been shortened and the dip of the HopeConway (403) source has been modified. The slip rates for all the multi-fault sources have been modified based on new information and to accommodate the new additions (i.e. maintaining the same cumulative slip rate at any given location along overlapping sources).

One new multi-fault source has been added to the suite of Jordan-Kekerengu-Needles-Chancet fault sources (Figure 9C) – a combination of the Papatea Fault, Jordan Thrust, and Kekerengu Fault (JorKekNeePap; 552). Modifications have also been made to the location of the existing JorKekCha (373) multi-fault source based on new mapping of the submarine Chancet Fault, and the JorKekNeed (374) and KekNeed (360) sources based on the location of the Needles Fault seabed rupture in the Kaikōura

earthquake. Slip rates have been modified to accommodate the new additions.

Conditional probability of rupture: Kekerengu, Hope, and Awatere faults

In the KSHM region, the two onshore active faults with the highest slip rates and shortest surface rupture earthquake recurrence intervals are the Kekerengu Fault and the Conway segment of the Hope Fault (see Supplement 1). Both faults have slip rates ≥20 mm/yr and recurrence intervals of just a few hundred years. The Kekerengu Fault last ruptured in the 2016 Kaikōura earthquake (CE 2016), while the Conway segment of the Hope Fault has not ruptured within the written historical period (i.e. within the last ~180 years) and may not have ruptured within the last ~300 years. Given the similar high average activity rates of these two faults (i.e. high slip rates and short recurrence intervals), but significantly different elapsed times since their respective most recent ruptures (i.e. for the Kekerengu Fault – since CE 2016, and for the Hope Fault – approaching its average recurrence interval of 180–300 years; Langridge et al. 2003), it was considered important for the KSHM to estimate time-dependent conditional probabilities of rupture for these two faults. The onshore fault with the next highest slip rate in the KSHM region, after the Kekerengu and Hope faults, is the northeast section of the Awatere Fault. This portion of the Awatere Fault last ruptured in CE 1848, and it was considered pertinent to estimate time-dependent conditional probabilities of rupture for this fault as well.

The basic statistical method adopted in this investigation for the estimation of conditional probabilities of rupture is that of Rhoades et al. (1994), with modifications described by Rhoades and Van Dissen (2003) and applied to the major onshore faults in the Wellington area by Rhoades et al. (2011) and Van Dissen et al. (2013). This modified method was also applied to specific faults included in the fault source model component of the Canterbury SHM (Gerstenberger et al. 2004, 2016). In the modified method, the probability of rupture of the fault in some future time-period of interest is expressed as a single value that accounts for both data and parameter uncertainties. A range of different recurrence-time models are considered – namely the exponential, lognormal, Weibull and inverse Gaussian (or Brownian passage-time) distributions.

The Rhoades and Van Dissen (2003) method requires knowledge of the distribution of the long-term average slip rate and its uncertainty, the mean single-event displacement and its uncertainty, and the dates of known recent ruptures and their uncertainties. It also requires specification of prior distributions for the parameters of the recurrence-time models. The prior distributions adopted here are constructed in the same way as in Rhoades and Van Dissen (2003), Rhoades et al. (2011), and Van Dissen et al. (2013) for the exponential, lognormal, Weibull, and inverse Gaussian models.

Input data

Table 1 lists the input data values for rupture timings, slip rate, and single-event displacement size, and their respective distributions, utilised in our evaluation of conditional probability of rupture of the Kekerengu

Table 1. Preferred distributions of input data for computation of conditional probability of rupture of the Kekerengu fault, Conway segment of the Hope fault, and northeast section of the Awatere fault.

	Probability distribution		
Fault characteristic	Kekerengu fault	Hope fault (Conway segment)	Awatere fault (northeast section)
Timing of past ruptures	Event I: CE 2016	Event I: uniform (CE 1840–1720)	Event I: CE 1848
	Event II: uniform (CE 1842–1701)	Event II: uniform (CE 1405–1295)	Event II: Trapezoidal (CE 990, CE 990, CE 970, CE 770)
	Event III: uniform (CE 1594–1422)	Event III: uniform (CE 1244–1163)	Event III: Trapezoidal (CE 970, CE 770, CE 350, CE 60)
	Event IV: uniform (CE 1047–701)		Event IV: Trapezoidal (CE 350, CE 60, BCE 2600, BCE 3350)
			Event V: Trapezoidal (BCE 2600, BCE 3350, BCE 3650, BCE 3650)
			Event VI: Trapezoidal (BCE 3960, BCE 3960, BCE 4540, BCE 4840)
			Event VII: Trapezoidal (BCE 4540, BCE 4840, BCE 6660, BCE 6660)
Horizontal slip rate (mm/year)	Uniform (20–26)	Normal (mean = 23, s.d. = 2)	Normal (mean = 6.0, s.d. = 0.4)
Mean single-event displacement (m)	Lognormal (mean = 9, CoV = 0.5)	Lognormal (mean = 5, CoV = 0.5)	Lognormal (mean = 5.3, CoV = 0.5)
Data sources	Litchfield et al. (2018) Van Dissen et al. (2005) Van Dissen et al. (2016) Kearse et al. (2018)	Langridge and Berryman (2005) Langridge et al. (2003) Langridge et al. (2013) Manighetti et al. (2015) Pope (1994) Van Dissen and Yeats (1991)	Benson et al. (2001) Hill et al. (2001) Little et al. (1998) Mason and Little (2006) Mason et al. (2006) This Study (Electronic Supplement 3.3)

Fault, Conway segment of the Hope Fault, and northeastern section of the Awatere Fault. Supplement 3 provides description and documentation of these value choices.

Conditional probability results

The estimated conditional probabilities of rupture of the Kekerengu Fault, Conway segment of the Hope Fault, and northeastern section of the Awatere Fault under each of the four recurrence-time distributions are shown for time intervals of 1, 5, 20, 50, and 100 years in Table 2, using the data input values and distributions listed in Table 1. The reader is referred to Rhoades and Van Dissen (2003) for details of the method, which is also summarised in Supplement 3. For the KSHM, a combined time-dependent result is derived for the three faults from the following weighted recurrence-time models: inverse Gaussian (0.5 wt), lognormal (0.3 wt), and Weibull (0.2 wt). This follows from the discussion presented in Van Dissen et al. (2013) and was also adopted for fault sources with conditional probability of rupture in the Canterbury SHM (Gerstenberger et al. 2014, 2016). The weighted result for each fault is listed in the respective 'combined time-dependent' rows of Table 2.

For the Kekerengu Fault, the current time-dependent hazard rate, represented by the combined model, is significantly lower – by more than an order of magnitude over the next 20 years – than the long-term average hazard rate, represented by the exponential model (Table 2; Figure 10). Although it does rise, the hazard rate for the Kekerengu Fault remains below half of the long-term average rate for the next 100 years. This is not surprising given that the fault last rupture in CE 2016 as part of the Kaikōura earthquake. For the Conway segment of the Hope Fault, the time-dependent hazard rate over the next 100 years is more than double the long-term hazard rate, which is represented by the exponential model. This reflects the fact that the most recent event occurred between 177 and 292 years ago and therefore, the elapsed time is now similar to the mean recurrence interval of about 330 years. For the northeast section of the Awatere Fault, the time-dependent hazard rate over the next 100 years is similar to, but slightly higher than, the long-term rate. This is, perhaps, somewhat surprising given that the fault has an average recurrence interval in the order of 1000 years and last ruptured only about 170 years ago but is probably a consequence of the large uncertainties in the timing of past rupture events for this fault (Table 2; Fig. ES 3.3.1) and the relatively large coefficient of variation (CoV) applied to its single-event displacement size. Both these factors combine together to 'allow' the Awatere Fault to take on a more random timing behaviour (i.e. the data allow for the possibility of very short as well as very long interevent times without a preference for intermediate ones), hence the similarity in results between the time-dependent models and the exponential model.

Proportioning probability to active fault earthquake sources

The conditional probabilities of rupture (and commensurate hazard rates and equivalent return

Table 2. Estimated conditional probability of rupture of the Kekerengu fault, Conway segment of the Hope fault, and northeast section of the Awatere fault during time intervals starting in CE 2017, allowing for uncertainties in data and parameter values.

		Time interval				
		1 yr	5 yr	20 yr	50 yr	100 yr
Kekerengu fault						
Recurrence-time distributions	Exponential	0.0029	0.014	0.056	0.13	0.25
	Lognormal	5.2×10^{-11}	2.9×10^{-6}	0.0011	0.019	0.10
	Weibull	7.9×10^{-4}	0.0047	0.024	0.072	0.17
	Inverse Gaussian	0	3.7×10^{-9}	5.4×10^{-4}	0.018	0.11
Combined time-dependent		1.6×10^{-4}	9.5×10^{-4}	0.0054	0.029	0.12
Annual hazard rate (events/year)		1.6×10^{-4}	1.9×10^{-4}	2.7×10^{-4}	5.9×10^{-4}	1.3×10^{-3}
Equivalent return time (years)		6250	5260	3690	1700	780
Hope fault (Conway segment)						
Recurrence-time distributions	Exponential	0.0030	0.015	0.058	0.14	0.26
	Lognormal	0.0071	0.035	0.13	0.30	0.50
	Weibull	0.0060	0.029	0.11	0.26	0.46
	Inverse Gaussian	0.0067	0.033	0.12	0.28	0.48
Combined time-dependent		0.0067	0.033	0.12	0.28	0.48
Annual hazard rate (events/year)		0.0067	0.0067	0.0064	0.0066	0.0065
Equivalent return time (years)		150	150	160	150	150
Awatere fault (northeast section)						
Recurrence-time distributions	Exponential	9.7×10^{-4}	0.0048	0.019	0.047	0.092
	Lognormal	0.0010	0.0051	0.021	0.055	0.12
	Weibull	0.0011	0.0056	0.023	0.056	0.11
	Inverse Gaussian	0.0011	0.0056	0.023	0.059	0.12
Combined time-dependent		0.0011	0.0055	0.022	0.057	0.12
Annual hazard rate (events/year)		0.0011	0.0011	0.0011	0.0012	0.0013
Equivalent return time (years)		910	910	900	850	780

Note: Input data from Table 1. The combined time-dependent conditional probability of rupture for each fault is derived from the following models with the following weights: inverse Gaussian (0.5 wt), lognormal (0.3 wt), and Weibull (0.2 wt). Also listed are the annual hazard rates, and equivalent return times of rupture of these faults based on the combined time-dependent conditional probability results.

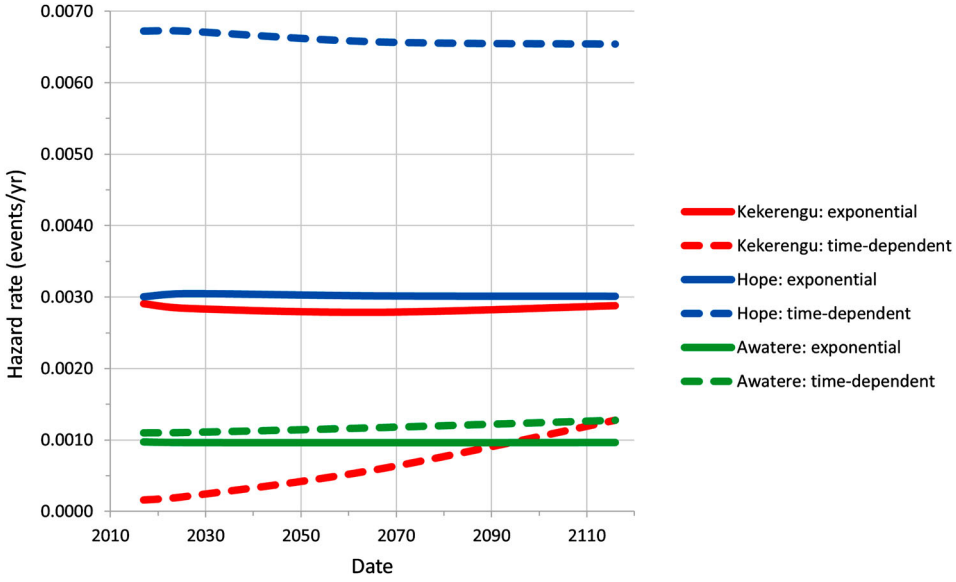

Figure 10. Comparison of hazard of rupture with time, from CE 2017–2117, of the Kekerengu fault, Conway segment of the Hope fault, and northeast section of the Awatere fault under the exponential recurrence-time distribution, and a combined time-dependent result derived from the following models with the following weights: inverse Gaussian (0.5 wt), lognormal (0.3 wt), and Weibull (0.2 wt)(see Table 2).

times) listed in Table 2 apply to the Kekerengu Fault, the Conway segment of the Hope Fault, or the northeast section of the Awatere Fault. However, in the KSHM, rupture of each of these faults is represented by multiple fault sources (Figure 9; Supplement 1). Table 3 lists the fault sources associated with each of the above three faults, and the percentage of the fault's total slip rate ascribed to each of the relevant active fault earthquake sources. In the KSHM, these slip rate percentages are used to proportion the combined time-dependent conditional probability results (including annual hazard rates) in Table 2 onto the individual fault sources, as shown in Table 3 and described in more detail in Supplement 3.

Hikurangi subduction interface

There are conflicting first-order views on the activity (seismogenic potential) of the Hikurangi subduction interface in the northeastern part of the South Island, and on its role during the M_w 7.8 Kaikōura earthquake. Previous research (e.g. Eberhart-Phillips and Bannister 2010; Eberhart-Phillips et al. 2014; Reyners et al. 2017) had suggested that the interface underlying northeastern South Island is locked and

Table 3. Proportioned annual hazard rates of rupture of the KSHM fault sources that encompass rupture of the Kekerengu fault, the Conway segment of the Hope fault, or the northeast section of the Awatere fault during time intervals starting in CE 2017.

		Time interval				
		1 yr	5 yr	20 yr	50 yr	100 yr
Kekerengu fault						
Annual hazard rate (events/year)		1.6×10^{-4}	1.9×10^{-4}	2.7×10^{-4}	5.9×10^{-4}	1.3×10^{-3}
KSHM Fault Source	% total slip rate	Proportioned annual hazard rate (events/year)				
KekNeed	9.1	1.5×10^{-5}	1.7×10^{-5}	2.5×10^{-5}	5.4×10^{-5}	1.2×10^{-4}
JorKekNeed	74.6	1.2×10^{-4}	1.4×10^{-4}	2.0×10^{-4}	4.4×10^{-4}	9.7×10^{-4}
JorKekNeedPap	2.7	4.3×10^{-6}	5.1×10^{-6}	7.3×10^{-6}	1.6×10^{-5}	3.5×10^{-5}
JorKekCha	13.6	2.2×10^{-5}	2.6×10^{-5}	3.7×10^{-5}	8.0×10^{-5}	1.8×10^{-4}
Hope fault (Conway segment)						
Annual hazard rate (events/year)		0.0067	0.0067	0.0064	0.0066	0.0065
KSHM Fault Source	% total slip rate	Proportioned annual hazard rate (events/year)				
HopeConway	93.5	0.0063	0.0063	0.0060	0.0062	0.0061
HopeConwayOS	4.1	2.8×10^{-4}	2.8×10^{-4}	2.6×10^{-4}	2.7×10^{-4}	2.7×10^{-4}
HopeConwayOSPap	2.4	1.6×10^{-4}	1.6×10^{-4}	1.5×10^{-4}	1.6×10^{-4}	1.6×10^{-4}
Awatere fault (Northeast section)						
Annual hazard rate (events/year)		0.0011	0.0011	0.0011	0.0012	0.0013
KSHM Fault Source	% total slip rate	Proportioned annual hazard rate (events/year)				
Awatere Northeast	37	4.1×10^{-4}	4.1×10^{-4}	4.1×10^{-4}	4.4×10^{-4}	4.8×10^{-4}
Awatere NE-Vernon	30	3.3×10^{-4}	3.3×10^{-4}	3.3×10^{-4}	3.6×10^{-4}	3.9×10^{-4}
Awatere NE-Vernon-Cloudy	33	3.6×10^{-4}	3.6×10^{-4}	3.6×10^{-4}	4.0×10^{-4}	4.3×10^{-4}

Note: Annual hazard rates for the Kekerengu, Hope and Awatere faults are from Table 2, and are proportioned to individual active fault earthquake sources according to the percentage of slip rate that specific fault source contributes to the total slip rate of either the Kekerengu fault, the Conway segment of the Hope fault, or the northeast section of the Awatere fault (see Supplement 1).

incapable of deformation in a large earthquake. In past seismic hazard models, this portion of the interface has not been included within the suite of earthquake sources representing rupture of the Hikurangi subduction interface (Stirling et al. 2012). However, more recent work – in particular investigations subsequent to the Kaikōura earthquake (e.g. Duputel and Rivera 2017; Wallace et al. 2017; Wen et al. 2017; Wang et al. 2018) – has highlighted the potential for this portion of the interface to fail in large earthquakes. In an attempt to accommodate these divergent opinions, an 11-person expert elicitation panel was convened, comprising seismologists, geodesists, and geologists. The panel was tasked with developing a parameterisation of Hikurangi interface rupture, including consideration of rupture (or not) of the interface south of Cook Strait. This parameterisation considered a range of available (published and unpublished) seismological, geological, paleoseismic and geodetic data.

Based on the weight of the evidence, the panel proposed a 50% weight for each of two branches of a Hikurangi interface source model logic tree. One branch utilises the 2010 NSHM Hikurangi interface sources, none of which involve rupture of the interface south of Cook Strait beneath northeastern South Island. The other branch extends the relevant 2010 NSHM Hikurangi interface sources southwestward past Cook Strait so as to underlie the northeastern South Island. This two-branch source model logic tree was adopted and applied to all hazard results in the KSHM.

The Hikurangi subduction sources from each of the two main branches of the logic tree are depicted in Figure 11. They are indicated as either: (1) '2010 Hikurangi subduction interface' for the branch utilising the earthquake sources defined in the 2010 NSHM (Stirling et al. 2012), or (2) 'extended Hikurangi subduction interface' for the branch that uses interface sources that have been extended south such that the plate interface would underlie the northeastern South Island. Each of the two main branches of the logic tree include several single – and multiple-segment sources (Table 4). Table 4 also lists key parameters such as M_w and recurrence interval for the various Hikurangi subduction interface earthquake sources used in the KSHM.

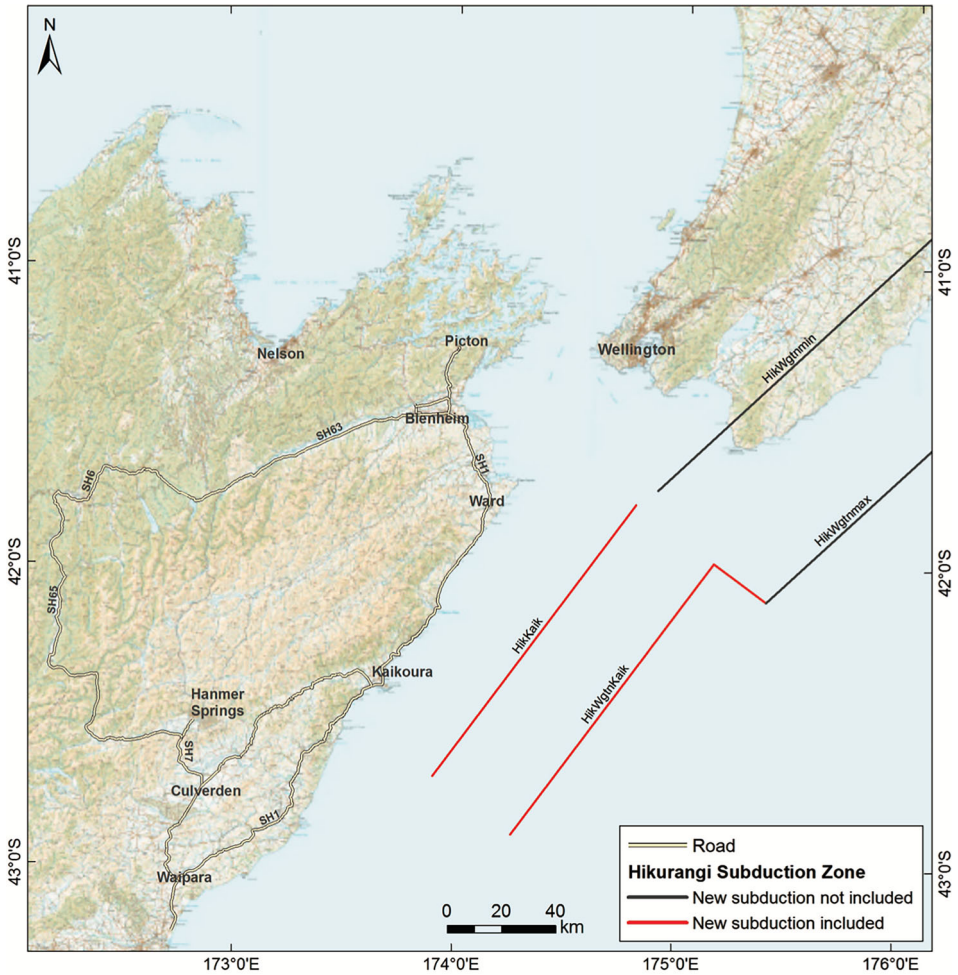

Figure 11. The extensions of the Hikurangi subduction interface sources from those of the 2010 NSHM (Stirling et al. 2012). The traces of the top edges of the new KSHM segments are shown in red, and those of 2010 NSHM sources in black. All sources dip at shallow angles to extend at depth under the land.

Ground motion characterisation

The ground motion prediction equations (GMPEs) that make up the second main component of the KSHM are used as part of a logic tree in order to better account for epistemic uncertainties in source modelling. The suite of GMPEs for each of the four tectonic region types in the source model (crustal, subduction interface, subduction intraslab, and volcanic) and their weights are shown in Table 5.

GMPE selection was based primarily on the analysis of GMPE performance by Van Houtte (2017) using New Zealand strong motion data (Van Houtte et al. 2017). For the volcanic, subduction interface, and subduction intraslab tectonic regimes the selected GMPEs and weights are those recommended by Van Houtte (2017). For crustal earthquakes, the recommended GMPEs have been modified from Van Houtte by including the McVerry et al. (2006) GMPE due to its long use with the NSHM (Stirling et al. 2002, 2012) and its use in developing the seismic hazard results that form the basis of Part 5 of the New Zealand structural design standard 1170 on earthquake design actions (Standards New Zealand 2004).

With the addition of the McVerry et al. GMPE, the weights recommended by Van Houtte (2017) for crustal GMPEs need to be redistributed. The general principle used by Van Houtte is to weight each of the NGA West-2 models (Abrahamson et al. 2014; Boore et al. 2014; Campbell and Bozorgnia 2014; Chiou and Youngs 2014) equally. However, since Van Houtte recommends the use of the New Zealand-modified Bradley (2013) GMPE which was derived from Chiou et al. 2010, he splits the Chiou and Youngs (2014) branch evenly with the New Zealand-modified Bradley (2013) model. In order to distribute the weights across the now five GMPEs, we have followed the overall principle of equal weights, giving the three NGA West-2 models of Abrahamson et al. (2014), Boore et al. (2014), and Campbell and Bozorgnia (2014) the weight of 0.2 each. The remaining 0.4 weight must then be distributed across the McVerry et al. (2006) and Chiou and Youngs/Bradley branches.

Other than the recommendations of the expert elicitation convened on the ongoing Canterbury earthquake sequence (Gerstenberger et al. 2014), there is little precedence to weight the two New Zealand GMPEs (McVerry et al. 2006; Bradley 2013) relative to one another. As such, the recommendations of that expert elicitation regarding epistemic uncertainty for M >= 5.5 were adopted for weighting branches of the GMPE logic tree with New Zealand models. This results in 60% of the remaining 0.4 weight given to the Chiou and Youngs/Bradley branch (0.26 weight in total, 0.13 to each GMPE) and 40% to the McVerry et al. (2006, p. 0.14 weight). The full GMPE logic tree and associated weights are presented in Table 5. Hazard results (Section 5) are the mean results of the GMPE and source model logic trees Tables 6 and 7.

Hazard calculations

All hazard calculations for the KSHM have been performed using the OpenQuake engine version 3.4 (Pagani et al. 2014). For the most part, the KSHM

Table 5. The GMPE logic tree used in the KSHM.

Tectonic regime	GMPE	Weight
Crustal	Abrahamson et al. (2014)	0.2
	Boore et al. (2014)	0.2
	Campbell and Bozorgnia (2014)	0.2
	Chiou and Youngs (2014)	0.13
	Bradley (2013)	0.13
	McVerry et al. (2006)	0.14
Volcanic	Bradley (2013)	0.5
	McVerry et al. (2006)	0.5
Subduction Interface	Atkinson and Boore (2003)	0.25
	McVerry et al. (2006)	0.25
	Zhao et al. (2006)	0.25
	Abrahamson et al. (2016)	0.25
Subduction Intraslab	Atkinson and Boore (2003)	0.25
	McVerry et al. (2006)	0.25
	Zhao et al. (2006)	0.25
	Abrahamson et al. (2016)	0.25

Table 4. Selected earthquake rupture parameters for the Hikurangi subduction interface sources in the 2010 NSHM[1] and extended Hikurangi subduction interface in the KSHM.

				Recurrence Interval (yrs)	
SOURCE	NSHM/KSHM	Length (km)	M_w	2010 NSHM[1]	Extended subduction interface
HikALL_NSHM	NSHM	620	9.0	6700	–
Wellington_Min	NSHM / KSHM	220	8.1	850	850
Wellington_Max	NSHM / KSHM	220	8.4	1600	1600
Hik_Kaikōura	KSHM	127	7.7	–	850
Hik_Wgn_Kaikōura	KSHM	347	8.2	–	1300
Hik_HBay_Min	NSHM / KSHM	200	8.1	1300	1300
Hik_HBay_Max	NSHM / KSHM	200	8.3	1700	1700
Hik_Rauk_Min	NSHM / KSHM	200	8.1	1000	1000
Hik_Rauk_Max	NSHM / KSHM	200	8.3	1400	1400
Hik_Kaikōura_ALL	KSHM	747	9.0	–	8500
Sum Annual rates				0.0051	0.0070
1/Sum (yrs)				200	140
New Kaikōura Sources (yrs)	KSHM			–	510

[1]Corrected from Stirling et al. (2012).
Note: The two branches are given equal weight in the logic tree.

Table 6. Unweighted horizontal acceleration hazard values (in units of g) at several locations in the South Island, corresponding to Class C Shallow Soil 1000 and 2500 years return periods at 1.0 s, using the Bridge Manual (NZTA 2016), 2010 NSHM source model and KSHM.

Location	1000-years (1.0s) bridge manual	1000-years (1.0s) 2010 NSHM source model	1000-years (1.0s) KSHM	2500-years (1.0s) bridge manual	2500-years (1.0s) 2010 NSHM source model	2500-years (1.0s) KSHM
Blenheim	0.51	0.68	0.97	0.71	1.00	1.40
Seddon	0.62	0.79	1.25	0.86	1.14	1.76
Kaikōura	0.65	1.05	1.34	0.90	1.49	1.87
Murchison	0.53	0.43	0.57	0.73	0.60	0.82
Hanmer Springs	0.85	1.20	1.54	1.18	1.71	2.11
Springs Junction	0.70	0.84	0.99	0.96	1.32	1.50

has been developed specifically for the needs of hazard modelling and standard probabilistic seismic hazard analysis (PSHA) practice. However, as in the Canterbury SHM, the clustering model component represents a fundamental change in how earthquake rates are estimated for hazard and is based on models that were developed with earthquake forecasting, and not hazard, as an end goal. Because of this, some extra steps are required in order to use the clustering model in PSHA. In this section we will discuss assumptions that have been made to allow the clustering model and the source model as a whole, including fault sources with conditional probability of rupture, to meet the needs of traditional hazard analyses and end-users.

Use of time-dependent rates on faults and poisson assumption

Most of the fault sources in the KSHM fault model are assumed to be Poissonian in nature, rupturing with some average recurrence interval. For the faults where sufficient data was available, conditional time-varying rates have been calculated as described in Section 3.3. These time-varying rates are then assumed to be Poissonian for the hazard calculations; this assumption introduces a bias to the hazard calculations. If we suppose a time-varying conditional probability of fault rupture is replaced by an equivalent Poisson rate λ for a time period T, in N simulations of the Poisson process with rate λT, the expected number of events is then $N\lambda T$. Let R denote the ratio of this expected number to its true value under the time-varying model. The Poisson sampling does not allow for the fact that after one event occurs during the time period of length T, the probability of a second event will be much reduced. We analyse the scenario where the probability is reduced to zero, to obtain an upper bound on the bias induced by the Poisson model. In the scenario, the probability P of one earthquake in time is $P = 1 - e^{-\lambda T}$, i.e. the same as the Poisson probability of at least one earthquake in time T. In this scenario, the N simulations are now N samples from a binomial distribution with probability P of success. The expected number of events is then NP. An upper bound for R is then given by:

$$R < \frac{N\lambda T}{NP} = \frac{\lambda T}{1 - \exp(-\lambda T)}. \quad (10)$$

For example, for the Hope Fault (Conway segment) over a period of 100 years, we have an equivalent rate of $\lambda = 0.0065\ \mathrm{yr}^{-1}$ for a forecast over $T = 100$ yr. Hence we obtain $R < 1.36$.

For this example, we get an expectation of 65 events in $N = 100$ samples in the Poisson model, and 48 events in the alternative binomial scenario. If Y is the ground motion with 1% probability of exceedance in 10,000 years, the error distribution for log$Y$ in a GMPE is sampled on average 65 times. Now $p = 1/65 = 0.0154$ corresponds to a (2-sided) standard normal deviate of $\delta_1 = 2.42$, whereas $p = 1/48 = 0.0208$ corresponds to a standard normal deviate of $\delta_2 = 2.31$. If the GMPE has a residual standard deviation of σ, then the ratio R_Y of the expected 1% in 100-year ground motion under the Poisson model to that under the true model is limited by:

$$R_Y < \frac{10^{\delta_1 \sigma}}{10^{\delta_2 \sigma}}. \quad (11)$$

Table 7. Ratios between the KSHM and 2010 NSHM source model of unweighted horizontal 1.0 s spectral accelerations for Class C Shallow Soil at several locations in the South Island and lower North Island, for return periods of 1000 and 2500 years.

Location	1000-years (1.0s) KSHM/ 2010 NSHM	2500-years (1.0s) KSHM/ 2010 NSHM
Blenheim	1.4	1.4
Seddon	1.6	1.5
Kaikōura	1.3	1.3
Murchison	1.3	1.4
Hanmer Springs	1.3	1.2
Springs Junction	1.2	1.1

Hazard results

Figure 12 illustrates that future hazard at 10% in 100 years probability is greatest along the Hope Fault and in coastal northeast Marlborough extending to Cook Strait. This primarily results from the high

conditional probability of future major earthquakes on the Hope Fault along all segments from the west at the junction with the Alpine Fault to Kaikōura. The zone of high hazard along the coast north of Kaikōura is largely driven by expected aftershock and clustered earthquake activity. A lower but significant level of hazard is associated with the Cloudy Bay area at the seaward end of the Wairau Fault, and along the Lewis Pass section of the alternative route. The alternative route is coincident with the Hope Fault for about 40 km westward of Hanmer Springs and represents a significant challenge to resilience of that highway network in that region. The hazard diminishes southward from the Hope Fault but remains above 0.8 g at 0.5 s period for 50 km along both SH1 and the alternative route and the so-called inland route where extensive deep-seated landslides occurred during the 2016 Kaikōura Earthquake.

Comparison with 2010 NSHM source model and recorded motions in past New Zealand and international earthquakes

For a first order understanding of the hazard results, we have compared various hazard maps based on the revised KSHM (e.g. Figure 5.1) to equivalent calculations using the source model from the 2010 NSHM (Stirling et al. 2012). To allow evaluation of the effect of the change in just the seismicity model, we have run the 2010 NSHM with the logic tree combination of GMPEs used in the KSHM for this project. The published 2010 NSHM in Stirling et al. (2012) used only the McVerry et al. (2006) GMPE, different from the 2010 NSHM results shown in this project.

We compared multiple probability levels (e.g. 1/1000 AEP, 1/2500 AEP, and 1/10,000 AEP – note these are also called 1000, 2500 and 10,000 years return periods in other parts of the text) for PGA, SA(0.5 s), and SA(2.0 s) and for site classes B and C. For all comparisons, the dominant features that changed were consistent.

The deviations of the KSHM from the 2010 NSHM source model can be broken down into those coming from two elements of the KSHM: (1) revised recurrence intervals on large crustal faults that account for the time since the last rupture on the fault (e.g. Rhoades and Van Dissen 2003) (Supplement 3); and (2) the earthquake clustering (i.e. distributed seismicity) model representing the hazard increase from aftershocks and earthquake clustering in space and time.

The highest hazard in the model comes in the region of the Hope Fault (Figure 12). For example, for Class B, 1/1000 AEP SA(0.5 s), the estimated accelerations, without magnitude-weighting, exceed 1.6 g at locations along the Hope Fault and reach accelerations as high as 1.8 g on part of the Hope Fault north of Kaikōura. This represents an increase in hazard of 1.2–1.4 times the estimate from the 2010 NSHM source model. This increase comes from all three elements mentioned above. The most significant increases in hazard, when compared to the 2010 NSHM, are in two regions with lower hazard than that of the Hope Fault that are dominated by the clustering model. These two regions include areas of increased aftershock activity that is anticipated to continue. The first region, in the northeast of the map, and off the coast from Cape Campbell, the Class B, 1/1000 AEP SA(0.5 s) estimated accelerations, without magnitude-weighting, exceed 1.4 g. This represents roughly an increase of more than 1.4 times over the 2010 NSHM results. This region has undergone extensive earthquake activity in recent years, including two M6.5 + earthquakes in 2013, and has been one of the most active parts of the Kaikōura aftershock sequence. The second region, to the south of Kaikōura, the hazard increases up to more than 1.6 times when

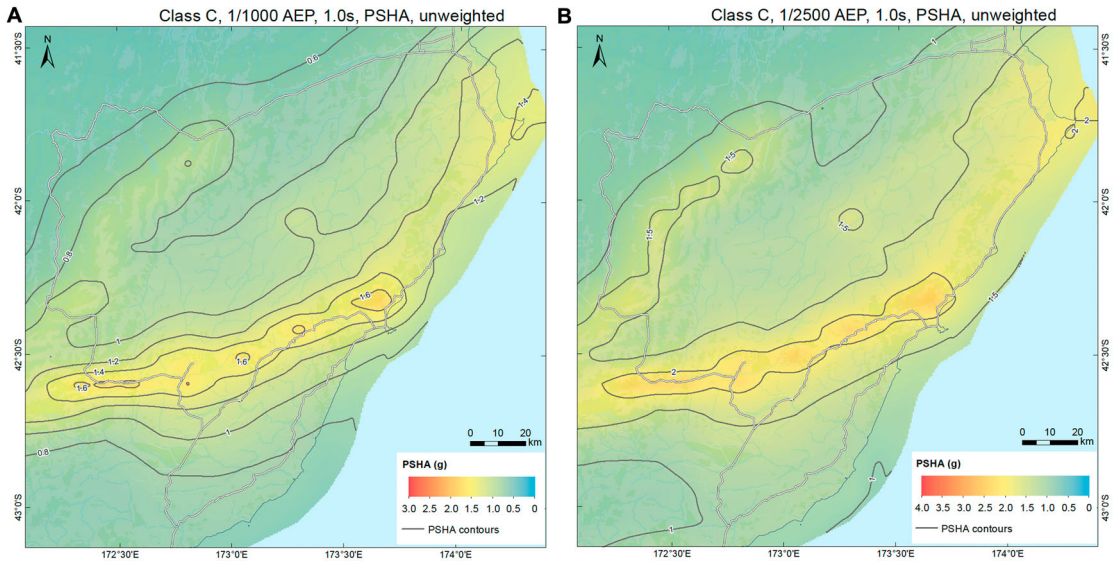

Figure 12. (Left) 1/1000 AEP SA(1.0s) hazard map for Site Class C. (Right) 1/2500 AEP SA(1.0s) hazard map for Site Class C.

compared to the 2010 NSHM source model, although the absolute hazard (1/1000 AEP, SA(0.5 s)) is lower than other areas, and ranges from 0.8 g to 1.2 g. In these two regions, the increases over the 2010 NSHM source model come from both the clustering model, and from the use of multiple GMPEs.

When estimating occurrence rates for Hope Fault segments, and other large faults in the region, we have made time-dependent estimates (using a clustering model) that take into account when the fault last ruptured. For the majority of the faults in the region, the time-dependent calculations increase the probability for earthquakes to occur in the next 100 years, and, hence, increase the estimated hazard. For the fault sources that ruptured in the Kaikōura earthquake, the probability for earthquakes to occur on those faults in the next 100 years has decreased. However, due to the use of the clustering model and multiple GMPEs the hazard has not decreased in most of these regions when compared to 2010 NSHM source model, despite the 2016 ruptures. Even along the Kekerengu Fault there is a slight increase in the SA (1.0 sec) hazard for site class C compared to the 2010 NSHM source model(Figure 13), although for some other hazard measures there is a slight decrease (Supplement 4). In this case, the probability of the fault rupturing in the next 100 years is strongly reduced, but the reduction is countered by an increased expectation of distributed seismicity in the vicinity of the fault – not of re-rupture of the fault itself – due to short-term and medium-term clustering. These two counteracting effects are always present in the aftermath of a major earthquake, but the important effects of clustering have often been overlooked in traditional seismic hazard analyses.

Earthquake hazard is estimated by combining the hazard contributions from all modelled sources in a region. When using GMPEs, the hazard estimate is dependent on multiple factors including the various magnitudes, rupture lengths, distances to the earthquake sources, spectral period, AEP, and so on. For this reason, the impact of the use of different GMPEs can vary significantly (e.g. increase or decrease), depending on where in the country they are applied, and what earthquake sources are contributing, etc. For the region in this study, the hazard is increased through the use of multiple GMPEs in a logic tree (Section 3.3.4).

It is also worth noting that the application of two different subduction zone models, one which does not rupture south of Cook Strait, and the other that does rupture as far south as Kaikōura, does not have a significant impact on the estimated hazard for the considerations of this study.

Hazard results from this study have also been compared to national and international strong-motion records from past earthquakes, as described below.

To understand the relevance of the estimated ground motions in the context of known New Zealand ground shaking observations, we have compared the maximum estimated 1/2500 and 1/10,000 AEP SA (1.0 s) and SA(2.0 s) accelerations to spectra from large shaking in past New Zealand earthquakes. In Figure 14 it can be seen that SA(1.0 s) accelerations from both AEPs have been exceeded in one or more earthquakes in New Zealand in the last 10 years. The 1/10,000 AEP SA(2.0 s) accelerations have not been exceeded in the past 10 years in New Zealand, but the 1/2,500 AEP have been matched or exceeded by 4 earthquakes during this time.

Additionally, we compared records from the Cosmos data set of international strong ground motion recordings from subduction earthquakes for the 46 years since 1971. For the SA (1.0 s) there are numerous

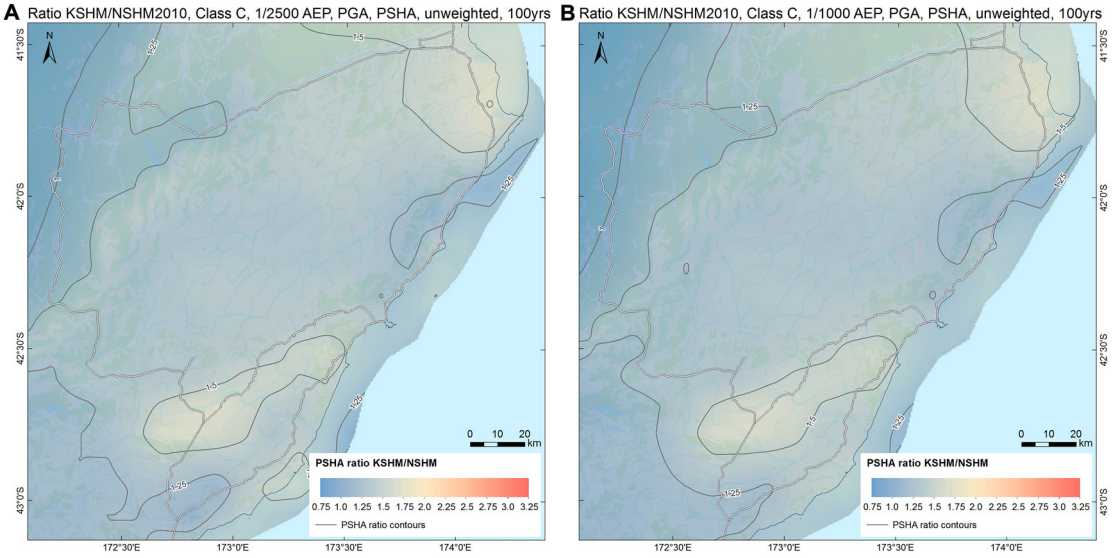

Figure 13. Ratios of 100 year hazard forecasts between KSHM hazard and Stirling et al. (2012) 2010 NSHM. (Left) 1/1000 AEP SA (1.0s) hazard map for Site Class C. (Right) 1/2500 AEP SA(1.0s) hazard map for Site Class C.

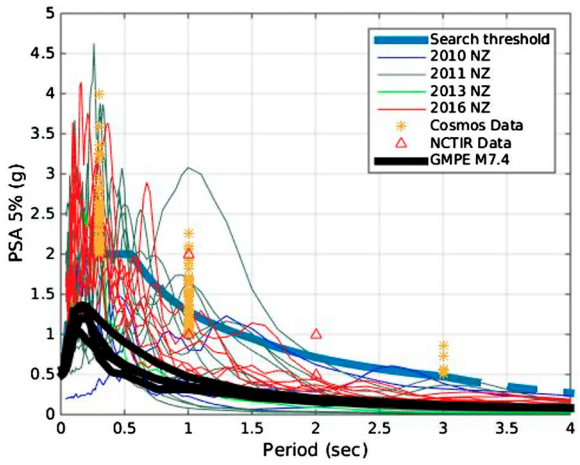

Figure 14. Compilation of NZ (thin lines) and international (stars) spectral accelerations (5% damping) with data points exceeding a predefined threshold level (thick blue line), NCTIR extreme values (2,500 and 10,000y – triangle) and mean of GMPE simulations for a M 7.4 earthquake for a site located at 1 km fault rupture distance (black lines).

exceedances of the 1/2,500 AEP acceleration and several at the 1/10,000 AEP. SA (2.0 s) accelerations are not available in this data set, but we have examined SA(3.0 s) which has several exceedances which suggest a similar result to what is seen at SA(2.0 s).

These comparisons with recorded accelerations from New Zealand and overseas illustrate that the levels of shaking derived in this study, while high, are certainly plausible.

Conclusions

Building on the work of the Canterbury SHM, we have implemented a time-dependent hazard model to inform roading and rail infrastructure recovery following the 2016 Kaikōura M7.8 earthquake. Similar to the Canterbury SHM, and different to many such hazard models, the KSHM was required to be built on a very short time frame so that it could inform the ongoing recovery. This was accomplished by building on what we had learned with the Canterbury SHM and from other forecasting work over the past 10 years.

An important difference from the KSHM and other recent time-dependent clustering models (Papadopoulos et al. 2020; Chioccarelli et al. 2021; Orlacchio et al. 2022) is the use of the EEPAS medium-term clustering model, and the use of the overall hybrid modelling framework. Both of these modelling components are influencing the current New Zealand NSHM revision for 2022.

Challenges remain for the use of such clustering-based time-dependent hazard models in application and decision making. Three of the key challenges are:

- Distilling a time-varying rate down to a single rate that can inform downstream decisions requiring a single metric (e.g. the KSHM applied a discount rate method to transform the time-varying rate);
- Engineering fragilities and loss vulnerabilities may be poorly constrained and ill-equipped to handle the high rates and accelerations coming from such a model;
- PSHA methods are reliant on a simplification for the rate calculation when calculating the probability of 1 or more events, losing the ability to understand the impact of, e.g. 2 or more, or 3 or more which can result from a clustering model (accounting for the cascading effect of sequence-based event-aftershocks).

Acknowledgements

We acknowledge the New Zealand GeoNet project and its sponsors EQC, GNS Science, LINZ, NEMA and MBIE for providing the earthquake catalogue data used in this study. Some of the research was undertaken for the North Canterbury Transport Infrastructure Recovery (NCTIR). The GNS Science Hazard and Risk Management Programme supported the preparation of the manuscript.

Disclosure statement

No potential conflict of interest was reported by the author(s).

Data availability statement

The earthquake catalogue data that support the findings of this study are available from the GeoNet website at https://quakesearch.geonet.org.nz/. The fault source parameters data supporting the findings of this study are available within the article and its supplementary materials.

Supplement 1 is available at Zenodo: https://zenodo.org/record/7340153#.Y45vx9JByXJ.
Supplements 2–4 are available at the GNS Science Dataset Catalogue:
Supplement 2, https://doi.org/10.21420/VRYT-VT95;
Supplement 3, https://doi.org/10.21420/Y8HV-GX02; and,
Supplement 4, https://doi.org/10.21420/83FE-H882.

Fault source locations are available on request.

ORCID

Elizabeth Abbott http://orcid.org/0000-0002-2330-0642
Annemarie Christophersen http://orcid.org/0000-0003-1467-1414
Ian Hamling http://orcid.org/0000-0003-4324-274X
Yoshi Kaneko http://orcid.org/0000-0003-2342-0131
Andy Nicol http://orcid.org/0000-0001-5181-1151
Mark W. Stirling http://orcid.org/0000-0002-2562-4675

References

Abrahamson N, Addo K, Atkinson G, Chiou B, Gregor N, Silva W, Youngs R. 2014. Ground motion characterization for the BC Hydro SSHAC Level 3 study. In:

Proceedings of Tenth US National Conference on Earthquake Engineering, Frontiers of Earthquake Engineering; 2014 Jul 21-25; Anchorage, Alaska. Oakland (CA): Earthquake Engineering Research Institute.

Abrahamson N, Gregor N, Addo K. 2016. BC hydro ground motion prediction equations for subduction earthquakes. Earthquake Spectra. 32(1):23–44.

Aki K, Richards PG. 1980. Quantitative seismology: theory and methods. Vol. 1. San Francisco: Freeman.

Ando R, Kaneko Y. 2018. Dynamic rupture simulation reproduces spontaneous multi-fault rupture and arrest during the 2016 Mw 7.9 Kaikoura earthquake. Geophysical Research Letters. 45:12875–12883. doi:10.1029/2018GL080550.

Atkinson G, Boore D. 2003. Empirical ground motion relations for subduction-zone earthquakes and their application to Cascadia and other regions. Bulletin of the Seismological Society of America. 93(4):1703–1729.

Bai Y, Lay T, Cheung KF, Ye L. 2017. Two regions of seafloor deformation generated the tsunami for the 13 November 2016, Kaikoura, New Zealand earthquake. Geophysical Research Letters. 44:6597–6606. doi:10.1002/2017GL073717.

Barnes PM, Ghisetti FC. 2016. Structure, late Quaternary slip rate and earthquake potential of marine reverse faults along the North Westland deformation front, New Zealand. New Zealand Journal of Geology and Geophysics. 59:157–175.

Barnes PM, Ghisetti FC, Gorman A. 2016. New insights into the tectonic inversion of North Canterbury and the regional structural context of the 2010-2011 Canterbury earthquake sequence, New Zealand. Geochemistry. Geophysics Geosystems. 17:324–345. doi:10.1002/2015GC006069.

Barnes PM, Ghisetti FC, Gorman AR, Bull JM, Cağatay MN, Woelz S, Mountjoy JJ, Lamarche G, Collins JA, Castellazzi C. 2015. Active submarine faulting in North Canterbury and eastern Marlborough, South Island, New Zealand. NIWA Client Report WLG2015-3, 72 pp.

Barnes PM, Lamarche G, Bialas J, Henrys S, Pecher I, Netzeband GL, Greinert J, Mountjoy J, Pedley K, Crutchley G. 2010. Tectonic and geological framework for gas hydrates and cold seeps on the Hikurangi subduction margin, New Zealand. Marine Geology. 272:26–48. doi:10.1016/j.margeo.2009.03.012.

Barrell DJA. 2013. General distribution and characteristics of active faults and folds in the Selwyn District, North Canterbury. GNS Science Consultancy Report 2012/325, 53 pp. https://api.ecan.govt.nz/TrimPublicAPI/documents/download/1811995.

Barrell DJA. 2015. General distribution and characteristics of active faults and folds in the Kaikōura District, North Canterbury. GNS Science Consultancy Report 2014/210, 59 pp. https://api.ecan.govt.nz/TrimPublicAPI/documents/download/1811995.

Barrell DJA, Begg JG. 2013. General distribution and characteristics of active faults and folds in the Waimakariri District, North Canterbury. GNS Science Consultancy Report 2012/326, 52 pp. https://api.ecan.govt.nz/TrimPublicAPI/documents/download/1811999.

Barrell DJA, Townsend DB. 2012. General distribution and characteristics of active faults and folds in the Hurunui District, North Canterbury. GNS Science Consultancy Report 2012/113, 30 pp. https://api.ecan.govt.nz/TrimPublicAPI/documents/download/1811995.

Barrell DJA, Van Dissen RJ. 2014. Assessment of active fault ground deformation hazards associated with the Ashley Fault Zone, Loburn, North Canterbury. GNS Science Consultancy Report 2013/173, 59 pp.

Beavan J, Haines J. 2001. Contemporary horizontal velocity and strain rate fields of the Pacific-Australian plate boundary zone through New Zealand. Journal of Geophysical Research. 106(B1):741–770.

Benson AM, Little TA, Van Dissen RJ, Hill N. 2001. Late Quaternary paleoseismic history and surface rupture characteristics of the eastern Awatere strike-slip fault, New Zealand. Geological Society of America Bulletin. 113:1079–1091.

Boore D, Stewart J, Seyhan E, Atkinson G. 2014. NGA-West2 equations for predicting PGA, PGV, and 5% damped PSA for shallow crustal earthquakes. Earthquake Spectra. 30(3):1057–1085.

Bradley BA. 2013. A New Zealand-specific pseudospectral acceleration ground-motion prediction equation for active shallow crustal earthquakes based on foreign models. Bulletin of the Seismological Society of America. 103(3):1801–1822. doi:10.1785/0120120021.

Bradley BA, Wotherspoon LM, Kaiser AE. 2017. Ground motion and site selection effect observations in the Wellington Region from the 2016 Mw 7.8 Kaikōura, New Zealand earthquake. Bulletin of the New Zealand Society for Earthquake Engineering. 50(2):94–105.

Campbell K, Bozorgnia Y. 2014. NGA-West2 ground motion model for the average horizontal components of PGA, PGV, and 5% damped linear acceleration response spectra. Earthquake Spectra. 30(3):1087–1115.

Chioccarelli E, Cito P, Visini F, Iervolino I. 2021. Sequence-based hazard analysis for Italy considering a grid seismic source model. Annals of Geophysics. 64(2):SE214. doi:10.4401/ag-8586.

Chiou B, Youngs R. 2014. Update of the Chiou and Youngs NGA model for the average horizontal component of peak ground motion and response spectra. Earthquake Spectra. 30(3):1117–1153.

Chiou B, Youngs RR, Abrahamson N, Addo K. 2010. Ground-motion attenuation model for small-to-moderate shallow crustal earthquakes in California and its implications on regionalization of ground-motion prediction models. Earthquake Spectra. 26:907–926.

Christophersen A, Rhoades DA, Gerstenberger MC, Bannister S, Becker J, Potter SH, McBride S. 2017. Progress and challenges in operational earthquake forecasting in New Zealand, in New Zealand Society for Earthquake Engineering Technical Conference, edited, New Zealand Society for Earthquake Engineering, Michael Fowler Centre, Wellington.

Clark KJ, Nissen EK, Howarth JD, Hamling IJ, Mountjoy JJ, Ries WF, Jones K, Goldstien S, Cochran UA, Villamor P, et al. 2017. Highly variable coastal deformation in the 2016 Mw7.8 Kaikōura earthquake reflects rupture complexity along a transpressional plate boundary. Earth and Planet Sci Lett. 474:334–344.

Console R, Rhoades DA, Murru M, Evison FF, Papadimitriou EE, Karakostas VG. 2006. Comparative performance of time-variant, long-range and short-range forecasting models on the earthquake catalogue of Greece. Journal of Geophysical Research. 111(B9):B09304. doi:10.1029/2005JB004113.

Duputel Z, Rivera L. 2017. Long-period analysis of the 2016 Kaikōura earthquake. Physics of the Earth and Planetary Interiors. 265:62–66. doi:10.1016/j.pepi.2017.02.004.

Eberhart-Phillips D, Bannister S. 2010. 3-D imaging of Marlborough, New Zealand, subducted plate and strike-slip fault systems. Geophysical Journal International. 182(1):73–96. doi:10.1111/j.1365-246X.2010.04621.x.

Eberhart-Phillips D, Bannister S, Ellis S. 2014. Imaging P and S attenuation in the termination region of the Hikurangi subduction zone, New Zealand. Geophysical Journal International. 198(1):516–536.

Evison FF, Rhoades DA. 2002. Precursory scale increase and long-term seismogenesis in California and northern Mexico. Annals of Geophysics. 45(3/4):479–495.

Evison FF, Rhoades DA. 2004. Demarcation and scaling of long-term seismogenesis. Pure and Applied Geophysics. 161(1):21–45.

Gerstenberger M, McVerry G, Rhoades D, Stirling M. 2014. Seismic hazard modeling for the recovery of Christchurch. Earthquake Spectra. 30(1):17–29. doi:10.1193/021913EQS037M.

Gerstenberger MC, Rhoades DA. 2010. New Zealand earthquake forecast testing centre. Pure and Applied Geophysics. 167(8/9):877–892. doi:10.1007/s00024-010-0082-4.

Gerstenberger MC, Rhoades DA, McVerry GH. 2016. A hybrid time-dependent probabilistic seismic-hazard model for Canterbury, New Zealand. Seismological Research Letters. 87(6):1311–1318.

Gerstenberger MC, Wiemer S, Jones L. 2004. Real-time forecasts of tomorrow's earthquakes in California: a new mapping tool. United States Geological Survey Open-File Report. 2004-1390.

Gerstenberger MC, Wiemer S, Jones LM, Reasenberg PA. 2005. Real-time forecasts of tomorrow's earthquakes in California. Nature. 435(7040):328–331.

Ghisetti FC, Johnston MR, Wopereis P. 2020. Structural evolution of the active Waimea-Flaxmore fault system in the Nelson-Richmond urban area, South Island, New Zealand. New Zealand J Geol Geophys. 63(2):168–189.

Hamling IJ. 2020. A review of the 2016 Kaikōura earthquake: insights from the first 3 years. Journal of the Royal Society of New Zealand. 50(2):226–244. doi:10.1080/03036758.2019.1701048.

Hamling IJ, Hreinsdóttir S, Clark K, Elliott J, Liang C, Fielding E, Litchfield N, Villamor P, Wallace L, Wright TJ, et al. 2017. Complex multifault rupture during the 2016 Mw 7.8 Kaikōura earthquake, New Zealand. Science. 356(6334). doi:10.1126/science.aam7194.

Harte DS. 2013. Bias in fitting the ETAS model: a case study based on New Zealand seismicity. Geophysical Journal International. 192(1):390–412.

Harte DS. 2015. Log-likelihood of earthquake models: evaluation of models and forecasts. Geophysical Journal International. 201(2):711–723.

Harte DS. 2016. Model parameter estimation bias induced by earthquake magnitude cut-off. Geophysical Journal International. 204(2):1266–1287. doi:10.1093/gji/ggv524.

Harte DS. 2019. Evaluation of earthquake stochastic models based on their real-time forecasts: a case study of Kaikoura 2016. Geophysical Journal International. 217(3):1894–1914. doi:10.1093/gji/ggz088.

Hill N, Little TA, Van Dissen RJ, Benson AM, Townsend DB, McLea B. 2001. A refined paleoseismic history of the eastern section of the Awatere Fault, New Zealand, based on results from a 2nd trench excavated near Lake Jasper. New Zealand Earthquake Commission Research Report. 97/262. https://www.eqc.govt.nz/resilience-and-research/research/search-all-research-reports/paleoseismicity-rates-of-active-deformation-and-structure-of-the-lake-jasper-pull-apart-basin-awatere-fault-new-zealand/.

Holden C, Kaneko Y, D'Anastasio E, Benites R, Fry B, Hamling IJ. 2017. The 2016 Kaikoura earthquake revealed by kinematic source inversion and seismic wavefield simulations: slow rupture propagation on a geometrically complex crustal fault network. Geophysical Research Letters. 44(22):11320–11328. doi:10.1002/2017GL075301.

Howell A, Nissen E, Stahl T, Clark K, Kearse J, Van Dissen R, Villamor P, Langridge R, Jones K. 2020. Three-dimensional surface displacements during the 2016 Mw 7.8 Kaikōura earthquake (New Zealand) from photogrammetry-derived point clouds. Journal of Geophysical Research: Solid Earth. 125. doi:10.1029/2019JB018739.

Jackson DD, Kagan YY. 1999. Testable earthquake forecasts for 1999. Seismological Research Letters. 70(4):393–403.

Kaiser A, Balfour N, Fry B, Holden C, Litchfield N, Gerstenberger M, D'Anastasio E, Horspool N, McVerry G, Ristau J, et al. 2017. The Kaikōura (New Zealand) earthquake: preliminary seismological report. Seismological Research Letters. 88:727–739. doi:10.1785/0220170018.

Kearse J, Little TA, Van Dissen RJ, Barnes P, Langridge R, Mountjoy J, Ries W, Villamor P, Clark K, Benson A, et al. 2018. Onshore to offshore ground-surface and seabed rupture of the Jordan–Kekerengu–Needles fault network during the 2016, Mw 7.8 Kaikōura earthquake, New Zealand. Bulletin of the Seismological Society of America. 108(3B):1573–1595. doi:10.1785/0120170304.

Langridge R, Campbell J, Hill N, Pere V, Pope J, Pettinga J, Estrada E, Berryman K. 2003. Paleoseismology and slip rate of the conway segment of the Hope fault at Greenburn Stream, South Island, New Zealand. Annals of Geophysics. 46:1119–1139.

Langridge RM, Almond PC, Duncan RP. 2013. Timing of late Holocene paleoearthquakes on the Hurunui segment of the Hope fault: implications for plate boundary strain release through South Island, New Zealand. Geological Society of America Bulletin. 125(5/6):756–775. doi:10.1130/B30674.1.

Langridge RM, Berryman KR. 2005. Morphology and slip rate of the Hurunui section of the Hope Fault, South Island, New Zealand. New Zealand Journal of Geology and Geophysics. 48:43–58.

Langridge RM, Ries WF, Litchfield NJ, Villamor P, Van Dissen RJ, Barrell DJA, Rattenbury MS, Heron DW, Haubrook S, Townsend DB, et al. 2016. The New Zealand active faults database. New Zealand Journal of Geology and Geophysics. 59:86–96.

Langridge RM, Rowland J, Villamor P, Mountjoy J, Townsend DB, Nissen E, Madugo C, Ries WF, Gasston C, Canva A, et al. 2018. Coseismic rupture and preliminary slip estimates for the Papatea fault and its role in the 2016 Mw 7.8 Kaikōura, New Zealand, earthquake. Bull Seismol Soc America. 108(3B):1596–1622.

Litchfield NJ, Morgenstern R, Van Dissen RJ, Langridge RM, Pettinga JR, Jack H, Barrell DJA, Villamor P. 2019. Updated assessment of active faults in the Kaikōura District. GNS Science consultancy report 2018/141. https://www.kaikoura.govt.nz/assets/App-4-CR2018-141-Active-Faults-Kaikoura-District-FINAL.PDF.

Litchfield NJ, Villamor P, Van Dissen RJ, Nicol A, Barnes PM, Barrell DJA, Pettinga JR, Langridge R, Little T, Mountjoy JJ, et al. 2018. Surface fault rupture of multiple crustal faults in the M_w 7.8 2016 Kaikōura, New Zealand,

earthquake. Bulletin of the Seismological Society of America. 108(3B):1496–1520. doi:10.1785/0120170300.
Little TA, Grapes R, Berger GW. 1998. Late Quaternary strike-slip on the eastern part of the Awatere fault, South Island, New Zealand. Geological Society of America Bulletin. 110:127–148.
Manighetti I, Perrin C, Dominguez S, Garambois S, Gauhemer Y, Malavielle J, Matteo L, Delor E, Vitard C, Beupretre S. 2015. Recovering paleoearthquake slip record in a highly dynamic alluvial and tectonic region (Hope fault, New Zealand) from airborne lidar. Journal of Geophysical Research. 120:4484–4509. doi:10.1002/2014JB011787.
Mason D, Little TA. 2006. Refined slip distribution and moment magnitude of the 1848 Marlborough earthquake, Awatere Fault, New Zealand. New Zealand Journal of Geology and Geophysics. 49:375–382.
Mason DPM, Little TA, Van Dissen RJ. 2006. Refinements of the paleoseismic chronology of the eastern Awatere Fault from trenches near Upcot Saddle, Marlborough, New Zealand. New Zealand Journal of Geology and Geophysics. 49(3):383–397.
McVerry GH, Zhao JX, Abrahamson NA, Somerville PG. 2006. New Zealand acceleration response spectrum attenuation relations for crustal and subduction zone earthquakes. Bulletin of the New Zealand Society for Earthquake Engineering. 39(1):1–58.
Mountjoy JJ, Barnes PM, Pettinga JR. 2009. Morphostructure and evolution of submarine canyons across an active margin: Cook Strait sector of the Hikurangi Margin, New Zealand. Marine Geology. 260:45–68. doi:10.1016/j.margeo.2009.01.006.
Mouslopoulou V, Saltogianni V, Nicol A, Oncken O, Begg J, Babeyko A, Cesca S, Moreno M. 2019. Breaking a subduction-termination from top-to-bottom: the 2016 Kaikōura earthquake. Earth and Planetary Science Letters. 506:221–223. doi:10.1016/j.epsl.2018.10.020.
New Zealand Treasury. 2020. Discount rates. [accessed 2022 June 29]. https://www.treasury.govt.nz/information-and-services/state-sector-leadership/guidance/financial-reporting-policies-and-guidance/discount-rates.
Nicol A, Robinson R, Van Dissen RJ, Harvison A. 2016. Variability of recurrence interval and single-event slip for surface-rupturing earthquakes in New Zealand. New Zealand Journal of Geology and Geophysics. 59(1):97–116.
Ogata Y. 1988. Statistical models for earthquake occurrences and residual analysis for point processes. Journal of the American Statistical Association. 83:9–27.
Orlacchio M, Cito P, Polidoro B, Villani M, Iervolino I. 2022. Sequence-based hazard maps for the United Kingdom. Bulletin of the Seismological Society of America. Seismological Society of America. doi:10.1785/0120210189.
Pagani M, Monelli D, Weatherill G, Danciu L, Crowley H, Silva V, Henshaw P, Butler L, Nastasi M, Panzeri L, Simionato M. 2014. Openquake engine: an open hazard (and risk) software for the global earthquake model. Seismological Research Letters. 85(3):692–702.
Papadopoulos AN, Bazzurro P, Marzocchi W. 2020. Exploring probabilistic seismic risk assessment accounting for seismicity clustering and damage accumulation: part I. Hazard analysis. Earthquake Spectra. 37:803–826. doi:10.1177/8755293020957338.
Pondard N, Barnes P. 2010. Structure and paleoearthquake records of active submarine faults, Cook Strait, New Zealand: implications for fault interactions, stress loading, and seismic hazard. Journal of Geophysical Research. 115:B12320. doi:10.1029/2010JB007781.
Pope JG. 1994. Secondary structures, Holocene displacements and paleoseismicity of the Conway segment of the Hope fault, Greenburn Stream to Sawyers Creek. Unpublished B.Sc. (Hons.). project, Geological Sciences Library, University of Canterbury, New Zealand.
Reyners M, Eberhart-Phillips D. 2009. Small earthquakes provide insight into plate coupling and fluid distribution in the Hikurangi subduction zone, New Zealand. Earth and Planetary Science Letters. 282:299–305. doi:10.1016/j.epsl.2009.03.034.
Reyners ME, Eberhart-Phillips D, Bannister SC. 2017. Subducting an old subduction zone sideways provides insights into what controls plate coupling. Earth and Planetary Science Letters. 466:53–61. doi:10.1016/j.epsl.2017.03.004.
Rhoades DA. 2007. Application of the EEPAS model to forecasting earthquakes of moderate magnitude in southern California. Seismological Research Letters. 78(1):110–115.
Rhoades DA. 2011. Application of a long-range forecasting model to earthquakes in the Japan mainland testing region. Earth Planets Space. 63(3):197–206. doi:10.5047/eps.2010.08.002.
Rhoades DA. 2013. Mixture models for improved earthquake forecasting with short-to-medium time horizons. Bulletin of the Seismological Society of America. 103(4):2203–2215. doi:10.1785/0120120233.
Rhoades DA, Christophersen A. 2017. Magnitude conversion of earthquake rate forecasts. Bulletin of the Seismological Society of America. 107(6):3037–3043. doi:10.1785/0120170225.
Rhoades DA, Christophersen A. 2019. Time-varying probabilities of earthquake occurrence in central New Zealand based on the EEPAS model compensated for time-lag. Geophysical Journal International. 219(1):417–429. doi:10.1093/gji/ggz301.
Rhoades DA, Christophersen A, Gerstenberger MC. 2015. Multiplicative earthquake likelihood models based on fault and earthquake data. Bulletin of the Seismological Society of America. 105(6):2955–2968. doi:10.1785/0120150080.
Rhoades DA, Christophersen A, Gerstenberger MC. 2017. Multiplicative earthquake likelihood models incorporating strain rates. Geophysical Journal International. 208:1764–1177. doi:10.1093/gji/ggw486.
Rhoades DA, Christophersen A, Gerstenberger MC, Liukis M, Silva F, Marzocchi W, Werner MJ, Jordan TH. 2018. Highlights from the first ten years of the New Zealand earthquake forecast testing center. Seismological Research Letters. 89(4):1229–1237.
Rhoades DA, Evison FF. 2004. Long-range earthquake forecasting with every earthquake a precursor according to scale. Pure and Applied Geophysics. 161(1):47–72.
Rhoades DA, Evison FF. 2005. Test of the EEPAS forecasting model on the Japan earthquake catalogue. Pure and Applied Geophysics. 162(6/7):1271–1290.
Rhoades DA, Evison FF. 2006. The EEPAS forecasting model and the probability of moderate-to-large earthquakes in central Japan. Tectonophysics. 417(1/2):119–130.
Rhoades DA, Gerstenberger MC. 2009. Mixture models for improved short-term earthquake forecasting. Bulletin of the Seismological Society of America. 99(2A):636–646. doi:10.1785/0120080063.

Rhoades DA, Liukis M, Christophersen A, Gerstenberger MC. 2016. Retrospective tests of hybrid operational earthquake forecasting models for canterbury. Geophysical Journal International. 204(1):440–456. doi:10.1093/gji/ggv447.

Rhoades DA, Schorlemmer D, Gerstenberger MC, Christophersen A, Zechar JD, Imoto M. 2011. Efficient testing of earthquake forecasting models. Acta Geophysica. 59(4):728–747.

Rhoades DA, Stirling MW. 2012. An earthquake likelihood model based on proximity to mapped faults and catalogued earthquakes. Bulletin of the Seismological Society of America. 102(4):1583–1599. doi:10.1785/0120110326.

Rhoades DA, Van Dissen RJ. 2003. Estimates of the time-varying hazard of rupture of the Alpine Fault, New Zealand, allowing for uncertainties. New Zealand Journal of Geology and Geophysics. 46(4):479–488.

Rhoades DA, Van Dissen RJ, Dowrick DJ. 1994. On the handling of uncertainties in estimating the hazard of rupture on a fault segment. Journal of Geophysical Research. 99(B7):13701–13712.

Schneider M, Clements R, Rhoades DA, Schorlemmer D. 2014. Likelihood- and residual-based evaluation of medium-term earthquake forecast models for California. Geophysical Journal International. 198(3):1307–1318. doi:10.1093/gji/ggu178.

Schorlemmer D, Gerstenberger MC. 2007. RELM testing center. Seismological Research Letters. 78(1):30–36.

Schorlemmer D, Gerstenberger MC, Wiemer S, Jackson DD, Rhoades DA. 2007. Earthquake likelihood model testing. Seismological Research Letters. 78(1):17–29.

Seebeck H, Van Dissen RJ, Litchfield NJ, Barnes PM, Nicol A, Langridge RM, Barrell DJA, Villamor P, Ellis SM, Rattenbury MS, et al. 2022. New Zealand Community Fault Model – version 1.0. Lower Hutt, N.Z.: GNS Science. GNS Science report 2021/57. 97 p. doi:10.21420/GA7S-BS61.

Standards New Zealand. 2004. NZS 1170.5:2004 - Structural design actions. Earthquake actions.

Stirling MW, McVerry G, Gerstenberger M, Litchfield N, Van Dissen R, Berryman K, Barnes P, Wallace L, Bradley B, Villamor P, et al. 2012. National seismic hazard model for New Zealand: 2010 update. Bulletin of the Seismological Society of America. 102:1514–1542.

Stirling MW, McVerry GH, Berryman KR. 2002. A new seismic hazard model for New Zealand. Bulletin of the Seismological Society of America. 92(5):1878–1903.

Utsu T, Ogata Y, Matsu'ura RS. 1995. The centenary of the Omori formula for a decay law of aftershock activity. Journal of Physics of the Earth. 43:1–33.

Van Dissen R, Rhoades DA, Little T, Litchfield N, Carne R, Villamor P. 2013. Conditional probability of rupture of the Wairarapa and Ōhariu faults, New Zealand. New Zealand Journal of Geology and Geophysics. 56(2):53–67. doi:10.1080/00288306.2012.756042.

Van Dissen R, Yeats RS. 1991. Hope fault, Jordan thrust, and uplift of the Seaward Kaikōura Range, New Zealand. Geology. 19:393–396.

Van Dissen RJ, Little T, Nicol A. 2005. Field trip 4: faults of eastern Marlborough: Picton, Awatere and Kekerengu, in Pettinga JR, Wandres AM, editors, Geological Society of New Zealand 50th Annual Conference, Kaikōura: Field Trip Guides, Geol. Soc. New Zeal. Misc. Publ. 119B, 85–110.

Van Dissen RJ, Little TA, Burke RM, Tonkin PJ, Norton KP, Bacon SN, Bowers R, Goldstein HL, Redwine JL, Sutherland DG, et al. 2016. Late Quaternary dextral slip rate of the Kekerengu Fault: New Zealand's third fastest on land fault. In: Riesselman C, Roben A, editors. Abstracts, GeoSciences 2016, Wanaka, Geoscience Society of New Zealand Miscellaneous Publication 145A. p. 89.

Van Houtte C. 2017. Performance of response spectral models against New Zealand data. Bulletin of the New Zealand Society for Earthquake Engineering. 50(1):21–38.

Van Houtte C, Bannister S, Holden C, Bourguignon S, McVerry G. 2017. The New Zealand strong motion database. Bulletin of the New Zealand Society for Earthquake Engineering. 50(1):1–20.

Wallace LM, Barnes P, Van Dissen R, Litchfield N, Mountjoy J, Langridge R, Lamarche G, Pondard N. 2012. The kinematics of a transition from subduction to strike-slip: an example from the central New Zealand plate boundary. Journal of Geophysical Research. 117: B02405. doi:10.1029/2011JB008640.

Wallace LM, Hreinsdóttir S, Ellis S, Hamling I, D'Anastasio E, Denys P. 2018. Triggered slow slip and afterslip on the southern Hikurangi subduction zone following the Kaikōura earthquake. Geophysical Research Letters. 45:4710–4718.

Wallace LM, Kaneko Y, Hreinsdóttir S, Hamling I, Peng Z, Bartlow N, D'Anastasio E, Fry B. 2017. Large-scale dynamic triggering of shallow slow slip enhanced by overlying sedimentary wedge. Nature Geoscience. 10 (10):765–770.

Wang T, Wei S, Shi X, Qiu Q, Li L, Peng D, Weldon RJ, Barbot S. 2018. The Kaikōura earthquake: simultaneous rupture of the subduction interface and overlying faults. Earth and Planetary Science Letters. 482:44–51.

Wen Y-Y, Ma K-F, Fry B. 2017. Multiple-fault, slow rupture of the 2016 M_w 7.8 Kaikōura, New Zealand earthquake: complementary insights from teleseismic and geodetic data. Bulletin of the Seismological Society of America. 108(3B):1774–1783.

Williams JN, Barrell DJA, Stirling M, Sauer KM, Duke GC, Hao KX. 2018. Surface rupture of the Hundalee Fault during the 2016 Mw 7.8 Kaikōura earthquake. Bulletin of the Seismological Society of America. 108(3B):1540–1555.

Woods RJ, McBride SK, Wotherspoon LM, Beavan S, Potter SH, Johnston DM, Wilson TM, Brunsdon D, Grace ES, Brackley H, Becker JH. 2017. Science to emergency management response: Kaikōura earthquakes 2016. Bulletin of the New Zealand Society for Earthquake Engineering. 50(2): 329–337.

Yeo GL, Cornell CA. 2005. Stochastic characterization and decision bases under time-dependent aftershock risk in performance-based earthquake engineering. PEER Report 2005/13, Pacific Earthquake Engineering Research Center, College of Engineering, University of California, Berkeley.

Zhao JX, Zhang J, Asano A, Ohno Y, Oouchi T, Takahashi T, Ogawa H, Irikura K, Thio H, Somerville P. 2006. Attenuation relations of strong ground motion in Japan using site classification based on predominant period. Bulletin of the Seismological Society of America. 96 (3):898–913.

Zinke R, Hollingsworth J, Dolan JF, Van Dissen R. 2019. Three-dimensional surface deformation in the 2016 Mw 7.8 Kaikōura, New Zealand, earthquake from optical image correlation: implications for strain localization and long-term evolution of the Pacific-Australian plate boundary. Geochemistry, Geophysics, Geosystems. 20:1609–1628. doi:10.1029/2018GC007951.